Clinical and Translational Report

Cell Metabolism

Ketosis Ameliorates Renal Cyst Growth in Polycystic Kidney Disease

Graphical Abstract

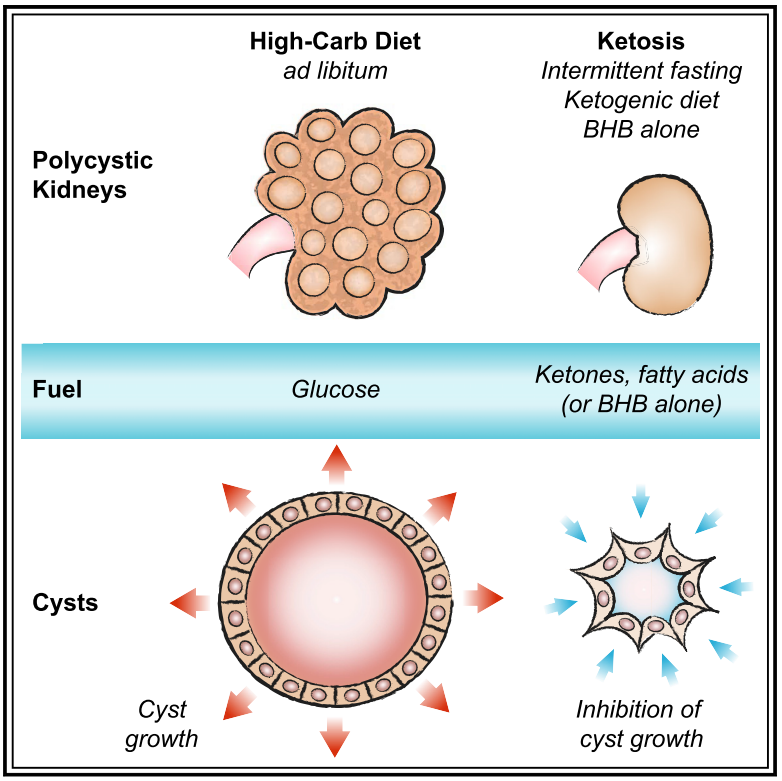

Highlights

- Ketosis prevents or reverses PKD in animal models
- Dietary changes that induce ketosis prevent PKD
- Oral β-hydroxybutyrate supplementation alone inhibits PKD progression
- Cystic cells are metabolically inflexible, which can be exploited for therapy

Authors

Jacob A. Torres, Samantha L. Kruger, Caroline Broderick, ..., Michal Mrug, Leslie A. Lyons, Thomas Weimbs

Correspondence

weimbs@ucsb.edu

In Brief

Dietary interventions that induce a state of ketosis were found to inhibit disease progression in animal models of polycystic kidney disease (PKD), a commonly inherited disease that leads to kidney failure. The beneficial effects of a ketogenic diet on PKD could be replicated in pre-clinical models by oral treatment with the natural ketone β-hydroxybutyrate.

Torres et al., 2019, Cell Metabolism *30*, 1007–1023
December 3, 2019
https://doi.org/10.1016/j.cmet.2019.09.012

CellPress

Cell Metabolism
Clinical and Translational Report

Ketosis Ameliorates Renal Cyst Growth in Polycystic Kidney Disease

Jacob A. Torres,[1] Samantha L. Kruger,[1] Caroline Broderick,[1] Tselmeg Amarlkhagva,[1] Shagun Agrawal,[1] John R. Dodam,[2] Michal Mrug,[3] Leslie A. Lyons,[2] and Thomas Weimbs[1,4,*]
[1]Molecular, Cellular, and Developmental Biology, and Neuroscience Research Institute, University of California, Santa Barbara, Santa Barbara, CA 93106-9625, USA
[2]Department of Veterinary Medicine & Surgery, College of Veterinary Medicine, University of Missouri, Columbia, MO 65211, USA
[3]Division of Nephrology, University of Alabama and the Department of Veterans Affairs Medical Center, Birmingham, AL, USA
[4]Lead Contact
*Correspondence: weimbs@ucsb.edu
https://doi.org/10.1016/j.cmet.2019.09.012

SUMMARY

Mild reduction in food intake was recently shown to slow polycystic kidney disease (PKD) progression in mouse models, but whether the effect was due to solely reduced calories or some other aspect of the diet has been unclear. We now show that the benefit is due to the induction of ketosis. Time-restricted feeding, without caloric reduction, strongly inhibits mTOR signaling, proliferation, and fibrosis in the affected kidneys in a PKD rat model. A ketogenic diet had a similar effect and led to regression of renal cystic burden. Acute fasting in rat, mouse, and feline models of PKD results in rapid reduction of cyst volume, while oral administration of the ketone β-hydroxybutyrate (BHB) in rats strongly inhibits PKD progression. These results suggest that cystic cells in PKD are metabolically inflexible, which could be exploited by dietary interventions or supplementation with BHB, representing a new therapeutic avenue to treat PKD.

INTRODUCTION

Autosomal dominant polycystic kidney disease (ADPKD) is a common genetic disease characterized by slowly progressive cyst growth in both kidneys, which leads to deterioration of renal function over the course of several decades, necessitating dialysis or kidney transplantation (Chebib and Torres, 2018; Cornec-Le Gall et al., 2019). Cysts derived from tubule epithelial cells exhibit changes in proliferation (Shillingford et al., 2006, 2010) and metabolism (Chiaravalli et al., 2016; Magistroni and Boletta, 2017; Padovano et al., 2017) and activation of signaling pathways that are normally dormant in healthy adult kidneys, such as mTOR and STAT signaling (Weimbs et al., 2013). ADPKD results from mutations in either the *PKD1* or *PKD2* genes, coding for polycystin-1 (PC1) and polycystin-2, respectively, but how these two proteins link to the many cellular changes observed within cyst-lining cells is still poorly understood (Ong and Harris, 2015).

A key signaling molecule activated in ADPKD is the kinase mTOR that regulates many cellular behaviors including proliferation, cell growth, and energy metabolism and is normally regulated by numerous inputs including growth factor signaling, cellular energy status, and nutrient availability (Cornu et al., 2013; Saxton and Sabatini, 2017). mTOR inhibitors, such as rapamycin, have proved highly effective in PKD rodent models (Ravichandran et al., 2014; Shillingford et al., 2006, 2010; Wahl et al., 2006) but unfortunately failed in clinical trials (Serra et al., 2010; Walz et al., 2010), most likely because high enough doses cannot be administered over the long term in humans due to significant extra-renal side effects and toxicities (Weimbs et al., 2018).

The high mTOR activity found in ADPKD may be related to recently observed changes in energy metabolism of renal cysts in animal models and in cultured cells that lack PC1. These mutant cells appear to exhibit an altered metabolism characterized by increased glycolysis and mitochondrial abnormalities, decreased oxidative phosphorylation, and defective fatty acid oxidation similar to the Warburg effect in cancer (Magistroni

Context and Significance

Polycystic kidney disease (PKD) is a common genetic disease that leads to kidney failure. Currently, the only approved treatment for this condition has only modest effects. However, calorie restriction was previously shown to inhibit disease progression in mouse models of PKD, but the mechanism remained unknown. Using mouse, rat, and cat models of PKD, Weimbs and colleagues now show that the metabolic state of ketosis is important for inhibiting PKD progression. They also show that simply adding the natural ketone β-hydroxybutyrate to a normal diet replicates the beneficial effects of a ketogenic regimen. These results suggest that cystic cells in PKD are metabolically inflexible, which can be exploited by a simple dietary intervention to provide a new therapy for PKD.

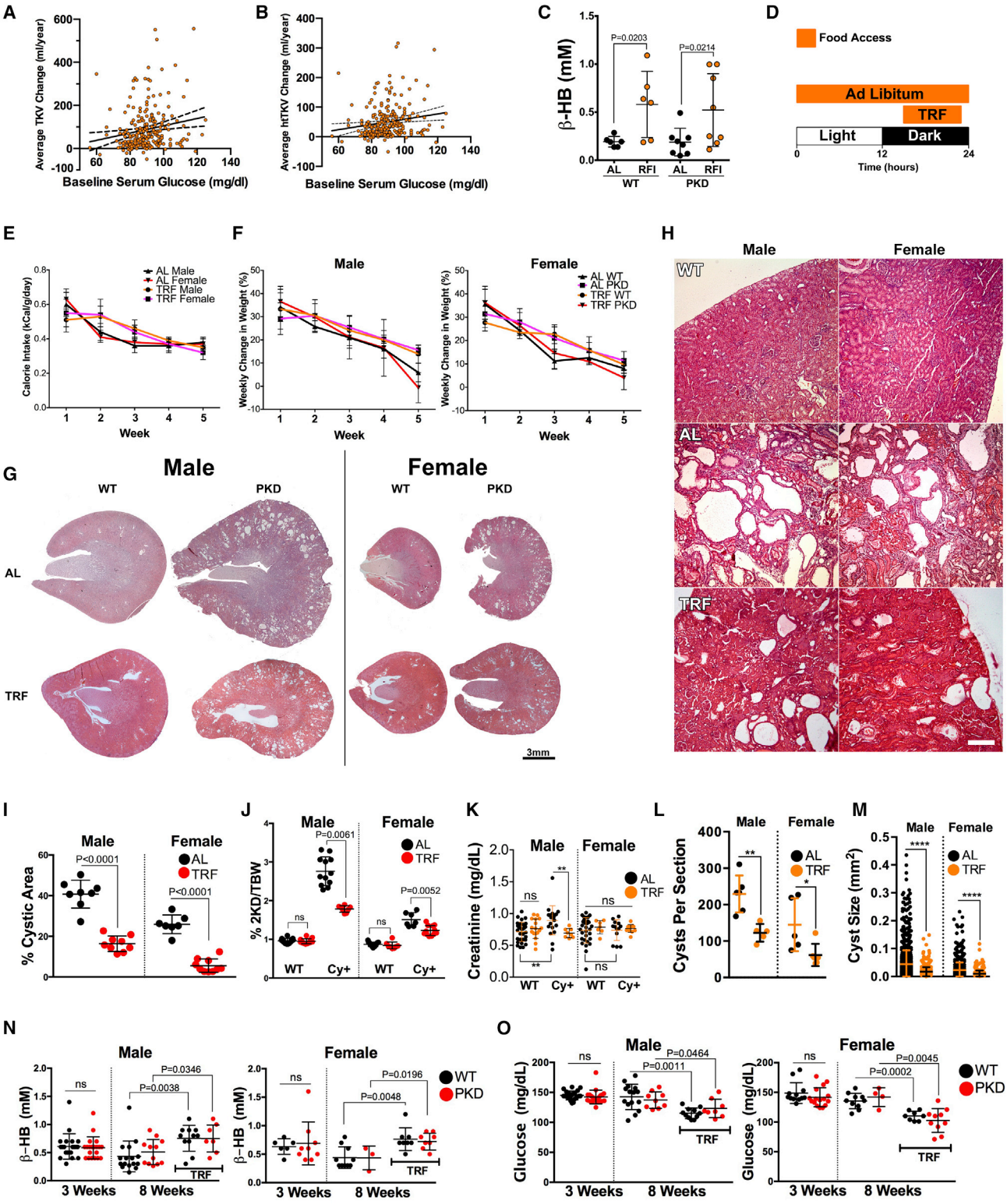

Figure 1. Serum Glucose Predicts TKV Increase in Individuals with ADPKD, and Time-Restricted Feeding Ameliorates PKD Disease Progression in a PKD Rat Model

(A and B) Linear regression analysis of the relationship between serum glucose levels (after overnight fasting) and average annual kidney volume change (TKV) (A) or height-adjusted TKV (htTKV) (B) in normoglycemic, non-diabetic individuals with ADPKD reveals positive correlation. Line represents best fit and dotted lines represent 95% confidence intervals.

(legend continued on next page)

and Boletta, 2017; Menezes et al., 2016; Rowe et al., 2013), making PC1-deficient cells apparently more dependent on glucose and gluconeogenic substrates like glutamine (Flowers et al., 2018; Hwang et al., 2015) in order to meet their energetic requirements. Similarly, abnormalities in mitochondria and energy metabolism can be triggered by mutations in the *PKD2* gene as well as the *PKHD1* gene, a principal gene mutated in autosomal recessive PKD (Chumley et al., 2018).Treatment of PKD cells and *Pkd1*-null mice with an inhibitor of glycolysis, 2-deoxyglucose (2DG), leads to a reduction in cyst growth (Chiaravalli et al., 2016; Riwanto et al., 2016). Similar effects on cyst growth have been observed utilizing other pharmacological interventions targeting metabolism including the AMPK activator metformin, the PPAR-α activator fenofibrate, the PPAR-γ activator rosiglitazone, and the GLS1 inhibitor BPTES (Weimbs et al., 2018).

As an alternative to pharmacological intervention, we considered influencing mTOR activity in the kidney through dietary intervention. Since mTOR is under control of nutrient availability, we recently investigated whether a reduction in food intake may affect renal cyst growth in an orthologous *Pkd1* mouse model (Kipp et al., 2016). Surprisingly, a very mild reduction in food intake, by only 23%, profoundly inhibited renal cyst growth and mTOR activity while not affecting body weight gain in these animals. An independent study, using two different orthologous mouse models, had the same conclusion and showed that food restriction by 40%, and even by only 10%, significantly inhibited renal cyst growth (Warner et al., 2016). These striking results raise questions about the mechanism underlying the beneficial effect of dietary restriction. Is the inhibition of renal cyst growth due to overall caloric restriction or due to the restriction of a particular macro- or micro-nutrient, or could it be caused by a different mechanism entirely?

We report here that dietary restriction strongly inhibits renal cyst growth due to metabolic changes caused by intermittent fasting. We show that time-restricted feeding, in comparison to isocaloric *ad libitum* feeding, causes an intermittent decrease of blood glucose and an increase in ketogenesis and leads to strong inhibition of renal cyst growth, proliferation, and fibrosis. These effects are not merely due to circadian feeding rhythm because *ad libitum* administration of a ketogenic diet (KD) similarly inhibits renal cyst growth. We show that acute fasting in mouse, rat, and feline models of PKD induces significant apoptosis in cyst-lining epithelial cells and a striking reversal of renal cystic burden. Finally, we show that supplementation of a normal chow (NC) diet with just the natural ketone β-hydroxybutyrate (BHB) replicates the beneficial effects of dietary restriction. Our results indicate that dietary restriction has profound inhibitory effects on PKD progression, and this depends on induction of ketosis, as renal cyst cells in PKD appear to be metabolically inflexible and thus unable to adapt to alternative fuel sources. These results are consistent with the observation that hyperglycemia and obesity correlate with faster disease progression in individuals with ADPKD. Our results strongly suggest that disease progression in ADPKD could be controlled by dietary interventions such as time-restriction or KDs and/or by BHB supplementation. These dietary interventions are safe for long-term use and well-established for the control of conditions such as type 2 diabetes, obesity, and childhood epilepsy, and so they could be adapted for the treatment of ADPKD.

RESULTS AND DISCUSSION

Glucose Levels Predict the Rate of Kidney Volume Change in Individuals with ADPKD

Individuals with ADPKD and type 2 diabetes have significantly larger total kidney volume (TKV) than those with ADPKD alone (Reed et al., 2012), and overweight or obesity associates with faster progression in early-stage ADPKD (Nowak et al., 2018). To investigate whether serum glucose levels even in normoglycemic, non-diabetic subjects with ADPKD correlate with disease progression, we explored this relationship in a cohort of individuals with ADPKD with preserved renal function that were recruited to the CRISP study (Yu et al., 2019). We used linear regression models to analyze average yearly change in TKV (average 87.8 mL/year, SD 99.2) and change in height-adjusted TKV (htTKV; average change 50.1 mL/m/year, SD 55.6) between baseline and the last follow-up with TKV and glomerular filtration rate (GFR) measurements (on average 9.7 years, SD 3.6 years) as a function of baseline serum glucose levels (after overnight fasting, average 89.6 mg/dL, SD 10.6), also adjusting for baseline TKV or htTKV and PKD gene mutation (*PKD1* versus *PKD2* versus no mutation detected). The baseline serum glucose in this cohort uniquely predicted a greater TKV (Figure 1A) and htTKV (Figure 1B) increase over time (for TKV change, n = 232, b = 0.95, p = 0.041; for htTKV change, b = 0.54, p = 0.042; Table

(C) Serum β-hydroxybutyrate (BHB) levels from PKD1$^{cond/cond}$:Nes^{cre} mice (PKD; n = 6) and wild-type controls (WT; n = 6) from our previous research (Kipp et al., 2016) on reduced food intake (RFI; n = 8) versus *ad libitum* (AL; n = 8) controls.
(D) Schematic outline of the feeding regimens used in this study. Time-restricted-fed (TRF) rats were allowed access to food from T14 to T22. Food access is indicated by the orange boxes.
(E) Average food intake per animal, per gram body weight, per week for rats on AL or TRF diet.
(F) Average change in body weight for male and female PKD and WT rats on AL or TRF diet.
(G and H) H&E-stained kidney sections. Scale bars represent 3 mm or 100 μm, respectively.
(I) Cystic index (percent cystic area) for rats on TRF or AL diet.
(J) 2-kidney weight to body weight ratios of TRF- and AL-treated rats.
(K) Serum creatinine levels of AL and TRF animals.
(L) Total number of cysts per kidney section in AL and TRF animals.
(M) Cyst sizes of cysts counted in (L).
(N) BHB levels at the start of the experiment (week 3) and the final time point of the experiment (week 8).
(O) Blood glucose levels at the start of the experiment (week 3) and the final time point of the experiment (week 8) (see also Figure S2).
Error bars represent SD. Statistical significance was determined using Mann-Whitney analysis. n = 8 male and 12 female Cy/+ rats; n =13 male and 8 female wild-type rats for TRF experiments. ****p < 0.0001, **p < 0.01.

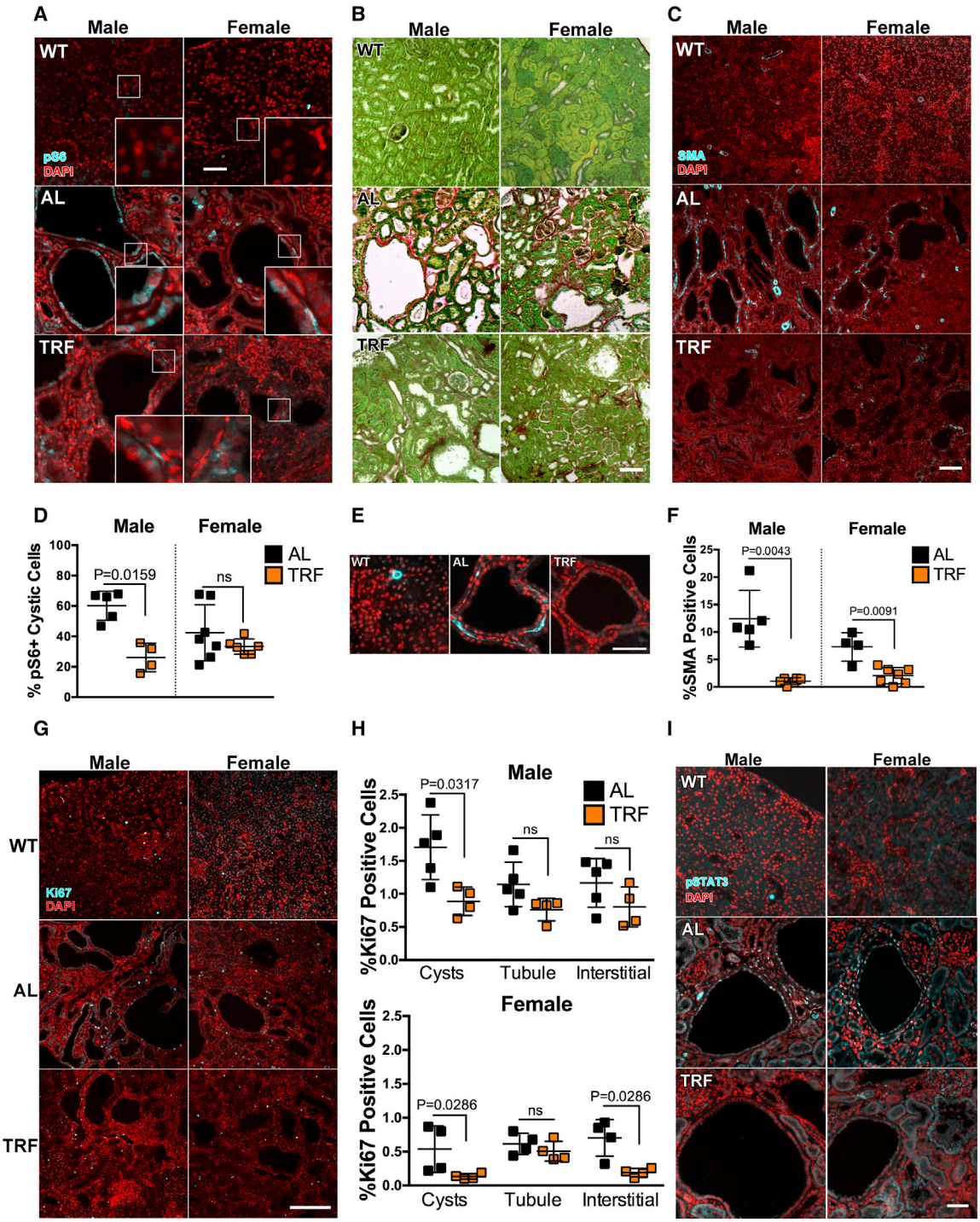

Figure 2. Time-Restricted Feeding Reduces mTORC1 Signaling, Fibrosis, and Proliferation in Cystic Kidneys

(A) Immunostaining of the mTORC1 marker pS6$^{S235/236}$(cyan), in kidneys from WT and PKD rats on AL diet (top and middle) or PKD rats on TRF diet (bottom).

(B) Sirius-red-stained kidney sections from AL and TRF rats showing collagen deposits (red).

(C) Immunostaining of the myofibroblast marker SMA (cyan), in kidneys from WT and PKD rats on AL diet (top and middle) or PKD rats on TRF diet (bottom).

(D) Quantification of pS6-positive cells in cyst-lining epithelia as a percent of the total number of DAPI-stained nuclei.

(E) Higher-magnification images of SMA-stained kidney sections showing pericystic myofibroblasts (cyan).

(F) Quantification of SMA-positive cells as the percent of total cells.

(G) Ki-67 immunostaining in kidneys from WT and PKD rats on AL diet (top and middle) or PKD rats on TRF diet (bottom).

(legend continued on next page)

S1). Similar analyses found no effect of the baseline serum glucose on average yearly change in GFR.

Together, these results suggest that glucose availability may directly affect renal cystic disease progression in ADPKD. This hypothesis is also supported by the previous findings that streptozotocin-induced hyperglycemia accelerates cystogenesis in a cilia-defective mouse model of PKD (Sas et al., 2015), and that glucose in the growth media promotes cyst growth in *in vitro* models (Kraus et al., 2016). Conversely, this hypothesis suggests that limiting glucose availability may ameliorate cystic progression in PKD.

Time-Restricted Feeding Ameliorates Disease Progression in the Han:SPRD Rat Model of PKD

We previously reported that a mild reduction in food intake (RFI) by 23% compared to *ad libitum*-fed (AL) controls strongly inhibits PKD progression in a mouse model of the disease (Kipp et al., 2016). In our study, we noticed a behavioral difference between animals in the RFI and AL cohorts. Whereas AL controls had continuous access to food that they consumed frequently, mice in the RFI cohort consumed their entire daily pre-weighed food allotment shortly after feeding, usually within 1 h. This behavioral difference makes it difficult to separate effects of caloric restriction and those of time-restricted feeding, in which animals are restricted from food for a set time period each day. We measured blood BHB levels from the animals in our previous RFI study and found significantly elevated levels in the RFI cohort compared to the AL cohort (Figure 1C), indicating that mice in the RFI group had indeed experienced intermittent fasting leading to ketosis.

To test whether the beneficial effect on renal cyst growth may be due to the effects of intermittent fasting, rather than reduced food intake per se, we placed Han:SPRD rats, a non-orthologous model of PKD with a mutation in *Anks6* (Brown et al., 2005), on a time-restricted feeding (TRF) regime wherein TRF animals had access to food for an 8-h period within their 12-h dark cycle (Figure 1D). Animals were treated for 5 weeks from post-natal weeks 3–8. This experimental time point was chosen because Han rat heterozygotes (Cy/+) exhibit rapid cystogenesis beginning at 3 weeks of age until around 8 weeks when cyst progression begins to slow. Male animals are more strongly affected than females in this model and exhibit very mild renal function impairment at 8 weeks (Cowley et al., 1993). Therefore, all outcomes were sex stratified. TRF animals consumed a comparable number of calories (Figure 1E) and gained weight similar to the AL controls (Figure 1F), indicating that TRF does not lead to food or caloric restriction. Similarly, there were no negative effects measured on any other organ (Figure S1, related to Figure 1). After 5 weeks of this dietary regimen, animals in the TRF cohort exhibited strikingly reduced renal cystic disease progression compared to animals in the AL cohort. Kidneys of TRF-treated animals were significantly less cystic (Figures 1G–1I) with a marked reduction in the 2-kidney/body weight ratio (Figure 1J) and improved kidney function as indicated by normalization of serum creatinine (Figure 1K). We next analyzed whole kidney sections for total cyst number (Figure 1L) and cyst size (Figure 1M), each of which were decreased in TRF animals compared to controls, indicating that TRF inhibited both cystogenesis and cyst expansion. Additionally, TRF-treated animals had increased levels of BHB (Figure 1N), indicating that the TRF regimen induced a state of ketosis. This was accompanied by reduced blood glucose (Figure 1O), which was consistently decreased at the end of the fasting period over the experimental time course (Figure S2, related to Figure 1).

TRF Reduces mTORC1 and STAT3 Signaling, Interstitial Fibrosis, and Proliferation in Cystic Kidneys

We assessed changes in known PKD associated pathways and pathologies. The kinase mTOR is important in nutrient sensation, and its activity is known to be elevated in PKD and is a driver of disease progression (Shillingford et al., 2010). We found a significant reduction in phosphorylated $S6^{S235/236}$ (Figures 2A and 2D), a downstream target in the mTOR pathway, in cyst-lining epithelial cells of TRF-treated male, but not female, Cy/+ animals indicating inhibition of mTORC1 activity. PKD also leads to interstitial fibrosis, a hallmark of progressive renal disease. We found that collagen deposition was markedly reduced in TRF compared to AL animals (Figure 2B). To determine whether the reduction of fibrosis may be due to a change in the myofibroblast population, we probed for the myofibroblast marker smooth muscle actin-1 (SMA). Whereas cysts in AL animals are associated with numerous SMA-positive myofibroblasts consistent with previous results (Norman, 2011; Song et al., 2017), myofibroblasts were strongly reduced, and frequently absent, in kidneys of TRF animals (Figures 2C, 2E, and 2F). Staining with the cell cycle marker Ki-67 revealed a significant reduction in cyst-lining cells in TRF compared to AL animals, indicating inhibition of proliferation (Figures 2G and 2H). We investigated STAT3 which has previously been shown to be activated in PKD and drives cystic progression (Leonhard et al., 2011; Takakura et al., 2011; Talbot et al., 2011, 2014; Torres et al., 2019; Weimbs et al., 2013). Active, phosphorylated STAT3 was reduced or absent in cysts in TRF-treated animals (Figure 2I).

A KD Ameliorates Disease Progression in Juvenile Han:SPRD Rats

To confirm that the observed beneficial effect of TRF on PKD kidneys is due to ketosis as opposed to other possible consequences of TRF, such as alterations in circadian rhythms, we explored the use of a KD. Han:SPRD rats were given *ad libitum* access to a high-fat, very-low-carbohydrate KD (caloric ratio of ~91% fat, ~2% carbohydrates, and ~5% protein) and compared to animals with *ad libitum* access to NC (caloric ratio of ~62% carbohydrates, ~25% protein, and ~13% fat). Animals were treated again for 5 weeks from post-natal weeks 3–8. Renal cystic disease progression was strongly inhibited in animals on

(H) Quantification of Ki-67-positive cells separated by location from the cyst lining, tubular, or interstitial regions and expressed as a percent of the total number of DAPI-stained nuclei.

(I) Immunostaining of pY-STAT3 (cyan), in kidneys from WT and PKD rats on AL diet (top and middle) or PKD rats on TRF diet (bottom).

Scale bars represent 100 μm. Error bars represent SD. Statistical significance determined using Mann-Whitney analysis. n = 8 male and 12 female Cy/+ rats; n =13 male and 8 female wild-type rats for TRF experiments.

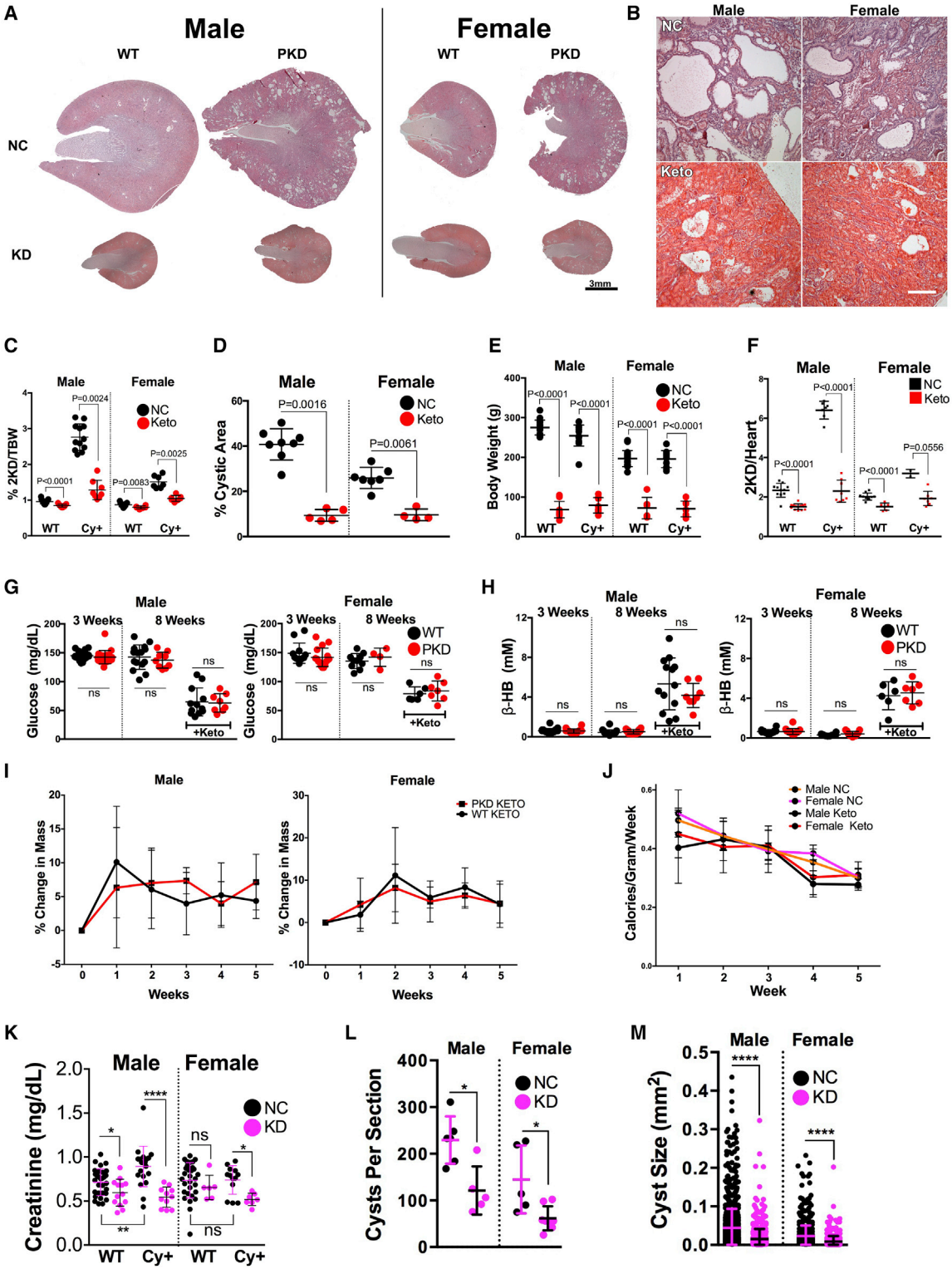

Figure 3. A Ketogenic Diet Ameliorates Disease Progression in Juvenile Han:SPRD Rats

(A) Low-magnification H&E images of WT or PKD rats fed *ad libitum* a normal chow (NC) or a ketogenic diet (KD). Scale bar represents 3 mm.

(B) High-magnification images of WT or PKD rats fed *ad libitum* a normal chow (NC) or a ketogenic diet (KD). Scale bar represents 100 μm.

(C) 2-kidney weight to body weight ratios of NC- and KD-treated rats.

(D) Cystic index (percent cystic area) from NC and KD cystic rats.

(E) Body weight of wild-type and cystic animals on NC and KD.

(legend continued on next page)

the KD regimen compared to those on NC (Figures 3A and 3B) along with a remarkable reduction in the 2-kidney to body weight (Figure 3C) and cystic area (Figure 3D). KD-treated rats exhibited decreased blood glucose (Figure 3G) and increased BHB levels (Figure 3H) compared to NC controls, and the level of ketosis was more profound than that achieved with the TRF regimen (Figure 1N). Animals on the KD appeared phenotypically normal and did not exhibit any signs of distress during the study. However, KD-treated animals exhibited reduced body weight gain (Figure 3E), and only gained approximately 2%–10% of their body weight each week during the study (Figure 3I). This lack of growth was not dependent on caloric intake, as the KD group consumed comparable calories to NC controls relative to their body weight (Figure 3J). Similar stunting induced by the commonly used ketogenic rodent chow has previously been described in juvenile rats (Liśkiewicz et al., 2018), which would normally be rapidly growing during the treatment period, and we attributed the stunting effect as most likely resulting from protein restriction. However, comparing effects of the KD on multiple organs (Figure S3, related to Figure 3) clearly showed that it has a disproportionate inhibitory effect on the growth of polycystic kidneys as compared to normal kidneys, for example, as illustrated after normalizing to heart weights (Figure 3F). Importantly, KD feeding led to improved kidney function (Figure 3K) as well as inhibited both cystogenesis (Figure 3L) and cyst expansion (Figure 3M).

The effects of KD treatment on PKD progression were generally similar to those caused by the TRF treatment. We found that mTOR (Figures 4A and 4E) and STAT3 (Figure 4B) activity in cystic epithelia were both blunted in KD-fed rats. SMA1-positive myofibroblasts were less in KD-fed animals compared to NC controls (Figures 4C and 4F), and this was accompanied by a decrease in collagen deposition (Figures 4D and 4G). A decrease in the percent of Ki-67-positive cells again suggests inhibition of cell cycle entry and proliferation (Figures 5H and 5I).

A KD is known to raise AMPK activity (Bae et al., 2016) and to promote fatty acid uptake by increasing expression of CPT1α via induction of PPARα (Grabacka et al., 2016). We found that KD feeding increased the levels of phospho-AMPK in the kidneys of cystic animals and increased CPT1α levels in male cystic, but not female cystic, rats (Figures 4J and 4K).

A KD Ameliorates Disease Progression in Adult Han:SPRD Rats

To exclude possible confounding factors related to the suppression of body weight gain, we next fed Han:SPRD rats at an older age (post-natal week 8–12) with a KD versus NC. At this age, there is no longer cystic kidney enlargement (Cowley et al., 1993), and we observed no further change in kidney size (compare Figures S3 and S4, related to Figure 5). The 4-week KD regimen resulted in effective ketosis, as illustrated by decreased blood glucose (Figure 5A) and increased blood BHB (Figure 5B).

During the treatment period, these adult rats only exhibit a modest body weight gain on NC (Figures 5C and 5D). While weight gain was mildly affected in rats on the KD, there was no difference between wild-type and cystic animals (Figures 5C and 5D). In contrast, the total mass of polycystic kidneys remained nearly the same in animals on NC but lowered by 35% in male rats on KD (Figure 5C), which was accompanied by diminished 2-kidney to body weight ratio (Figure 5G) and percent cystic area (Figure 5H). Similar to what was found in our juvenile experiments (Figure S3), the KD again affected the organ size of polycystic kidneys disproportionally because wild-type kidneys or other organs, such as the heart, were largely unaffected (Figures 5C, 5D, and S4). Unlike our juvenile experiments, serum creatinine was unaffected by KD treatment in adult rats (Figure 5I), as well as the total number of cysts per animal (Figure 5J). There was, however, a marked reduction in cyst size (Figure 5K), indicating that KD feeding prevents cyst growth in animals at that age. It should be noted that the number of cysts in untreated 12-week animals are similar to those in untreated 8-week animals (Figures 1L and 3M), indicating that there are few or no new cysts formed after 8 weeks of age. KD feeding led to a reduction in fibrosis in male animals, as indicated by reduced collagen (Figures 5L and 5P), but there was no detectable difference in myofibroblasts (Figures 5M and 5Q), mTOR activity (Figure 5N), or the cell cycle marker Ki-67 (Figures 5O and 5R).

Acute Fasting Leads to Cell Death and Renal Cyst Regression in Multiple PKD Animal Models

The strong inhibitory effects on PKD progression that we observed with ketosis induced by TRF and KD regimens occurred during the course of several weeks. To investigate whether ketosis has any fast-acting effects on renal cysts, we subjected Han:SPRD rats to acute ketosis via fasting. 8-week-old animals were fasted for 48 h with free access to water. As expected, acute fasting led to decreased blood glucose (Figure 6A) and increased blood BHB values (Figure 6B), indicating the induction of ketosis. The fasting-induced modest decrease in body weight (~12%) is expected due to depletion of fat and glycogen reserves, primarily in adipose tissue, liver, and skeletal muscle, respectively, and was consistent between wild-type and cystic animals (Figure 6C). Consequently, liver weights lowered among all groups (Figure S5, related to Figure 6). Strikingly, acute fasting strongly affected cystic kidneys, leading to a ~20% reduction in cystic area (Figure 6D) and a concurrent reduction in kidney mass (Figure 6E) and the 2-kidney/heart

(F) 2-kidney weight to heart weight ratios of NC- and KD-treated rats.
(G) Blood glucose at initial (week 3) and final time point (week 8) of the experiment.
(H) Blood β-hydroxybutyrate levels at initial (week 3) and final time point (week 8).
(I) Percent change in mass of KD-treated rats.
(J) Calories consumed per gram of body weight per week.
(K) Serum creatinine.
(L) Total number of cysts per kidney section.
(M) Cyst sizes of cysts counted in (L).
Error bars represent SD. Statistical significance determined from Mann-Whitney analysis. n = 8 male and 7 female Cy+ rats; n =13 male and 6 female wild-type rats for ketogenic diet experiments (*$p < 0.05$, ****$p < 0.0001$).

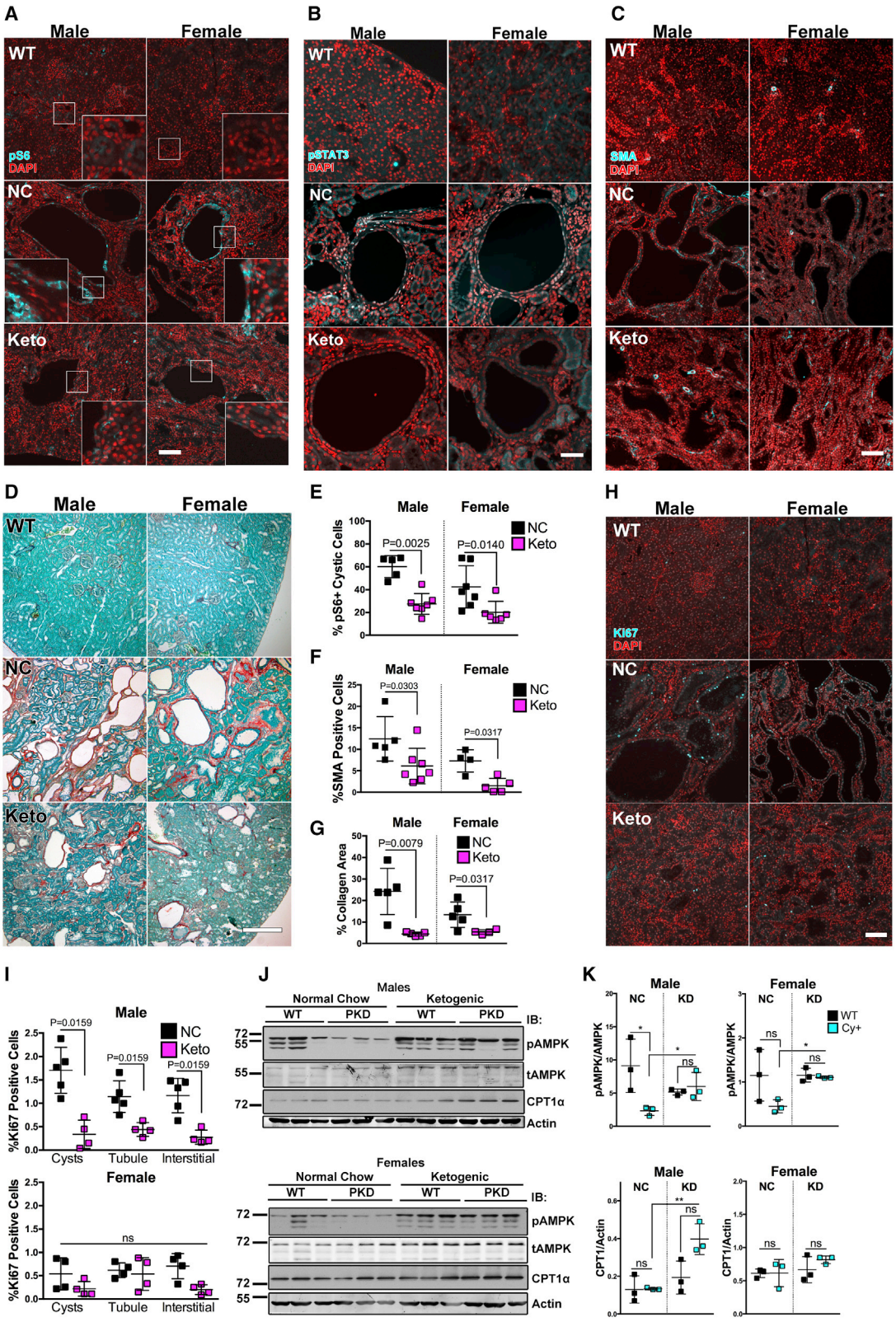

Figure 4. The Ketogenic Diet Reduces Markers of PKD in Juvenile Han:SPRD Rats

(A) Immunostaining of the mTORC1 marker pS6$^{S235/236}$(cyan), in kidneys from WT and PKD rats on normal chow diet (NC, top and middle) or PKD rats on ketogenic diet (KD) (bottom).

(legend continued on next page)

weight ratio (Figure 6F). Fasting had minimal-to-no effect on the weight of hearts (Figure 6G) and normal kidneys (Figure 6E) as expected, indicating that the effect of fasting is specific to PKD kidneys. The loss of mass was not due to any loss of glycogen because neither normal kidneys nor polycystic kidneys contain a significant amount of glycogen (Gatica et al., 2015). Instead, the extent of the reduction of cystic volume almost precisely accounted for the observed loss in kidney mass, suggesting that acute fasting leads to a loss of cyst fluid.

TUNEL staining revealed that acute fasting led to greater cell death of cystic cells (Figures 6H and 6I) but did not cause greater cell death in normal, non-cystic kidneys (Figure 6H). In particular, there was a conspicuous number of TUNEL-positive, detached cells in cyst lumens, indicating that these dead cells originated from sloughed-off cyst-lining cells (Figures 6H and 6I). Renal cysts in fasted animals frequently exhibited fragmented cells and denuded epithelium, which was not observed in renal cysts of control-fed cystic animals (Figure 6J). These results suggest that the loss of cyst fluid caused by acute fasting is due to cell death and disruption of the epithelial barrier of cysts leading to draining of cyst fluid presumably via the interstitium and lymphatics, leading to overall shrinking of polycystic kidneys.

To explore a possible reason for the induction of cell death of cystic cells by acute fasting, we considered the possibility that the increased supply of fatty acids during ketosis may affect cystic cells. As expected, intracellular oil droplets are rarely observed in normal or cystic kidneys in control-fed animals (Figure 6K). In contrast, acute fasting leads to accumulation of oil droplets in tubule cells in normal kidneys consistent with previous reports (Krzystanek et al., 2010; Scerbo et al., 2017). Cyst-lining cells in polycystic kidneys, however, exhibited a much exaggerated degree of cytoplasmic oil droplet accumulation (Figure 6K). Frequently, most of the cytoplasm of the affected cells appeared to be occupied by oil droplets suggesting a state of severe steatosis. These findings suggest that cyst-lining cells have the ability to take up circulating fatty acids during acute fasting but are unable to sufficiently metabolize them, which may lead to lipotoxicity and greater observed cell death.

To test whether acute ketosis due to fasting has similar effects in an orthologous mouse model of PKD, we used the previously described orthologous *Pkd1*:Nestin-Cre model (Kipp et al., 2016, 2018; Shillingford et al., 2010). Due to the smaller body size and faster metabolism of mice, we were only able to fast mice for 24 h as opposed to the 48 h in the rat model above. Fasting for 24 h, with free access to water, led to a pronounced decrease in blood glucose (Figure 6L) and increase in blood BHB (Figure 6M) but no significant change in kidney mass (Figure 6N) or 2-kidney to body weight (Figure 6O). However, TUNEL staining revealed that acute fasting again induced apoptotic cell death in cyst-lining cells and greater TUNEL-positive luminal cells, in polycystic kidneys but not in normal kidneys (Figures 6P and 6Q). We speculate that the short duration of fasting in mice is insufficient to lead to significant cyst draining and a measurable effect on cystic burden, as compared to rats.

To investigate whether these dramatic effects of acute fasting may extend to a non-rodent model of ADPKD, we employed a feline model in a longitudinal study. A naturally occurring mutation in the orthologous *PKD1* gene leads to a high prevalence of ADPKD in cats of Persian cat descent (Lyons et al., 2004). This feline model of ADPKD is arguably the model that most closely approximates human ADPKD because the underlying genetics appear to be identical. In contrast to most genetically engineered animal models, only one allele of the *PKD1* gene is affected in the germline in cats which presumably leads to a similar second-hit mechanism as in human ADPKD. Due to heterogeneity in the strain background, the rate of disease progression in feline ADPKD is naturally as variable as in human ADPKD, which necessitates a longitudinal study design. The trial included four adult cats with confirmed polycystic kidneys and *PKD1* DNA mutation, two males and two females, and one of each sex was desexed. The four cats had varying levels of renal cystic disease as shown by computed tomography (CT) (Figure S6, CT of PKD cats, related to Figure 6R; Table S3, related to Figure 6S) but no evidence of renal functional impairment. Animals were subjected to fasting for 72 h with free access to water. TKVs were determined from CT scans ~1.5 years prior to the study, immediately prior to and immediately after fasting. Cats lost between 0 and 0.3 kg of body weight, as would be expected due to loss of glycogen and fat deposits. Remarkably, the TKV values of all four cats decreased during the 72-h fasting periods by an average of 15% (range 3.5%–29.5%; Figure 6S). In contrast, the TKV values had increased or remained stable during the ~1.5 years prior to the study with an average increase of 1.2 mL/months (range −0.1 to + 2.8 mL/mo; Figure 6S). Fasting led to substantially reduced size of some of the identifiable cysts (Figure 6R, asterisk), suggesting that fluid draining occurred similar to what we observed in the rat model.

Oral BHB Treatment Prevents Polycystic Disease Progression in Juvenile Rats

We hypothesized that BHB itself may contribute to the observed inhibitory effect of ketosis on PKD progression. Recent results indicate that BHB not only is an energy source for cells but has complex effects on cellular signaling and metabolism that are

(B) Immunostaining of pY-STAT3 (cyan).
(C) Immunostaining of the myofibroblast marker SMA (cyan). Scale bars represent 100 μm.
(D) Sirius red/Fast Green-stained kidney sections showing collagen deposits (red). Scale bar represents 300 μm.
(E) Quantification of pS6-positive cells in cyst-lining epithelia as a percent of the total number of DAPI-stained nuclei in cysts.
(F) Quantification of SMA-positive cells as a percent of the total number of cells.
(G) Quantification of collagen-positive area.
(H) Ki-67 immunostaining. Scale bar represents 100 μm.
(I) Quantification of Ki-67-positive cells separated by location from the cyst lining, tubular, or interstitial regions and expressed as a percent of the total number of DAPI-stained nuclei.
(J) Immunoblot for the indicated markers.
(K) Quantification of immunoblots. Error bars represent SD. Statistical significance determined using Mann-Whitney analysis. n = 8 male and 7 female Cy+ rats; n =13 male and 6 female wild-type rats for ketogenic diet experiments (*$p < 0.05$, **$p < 0.01$).

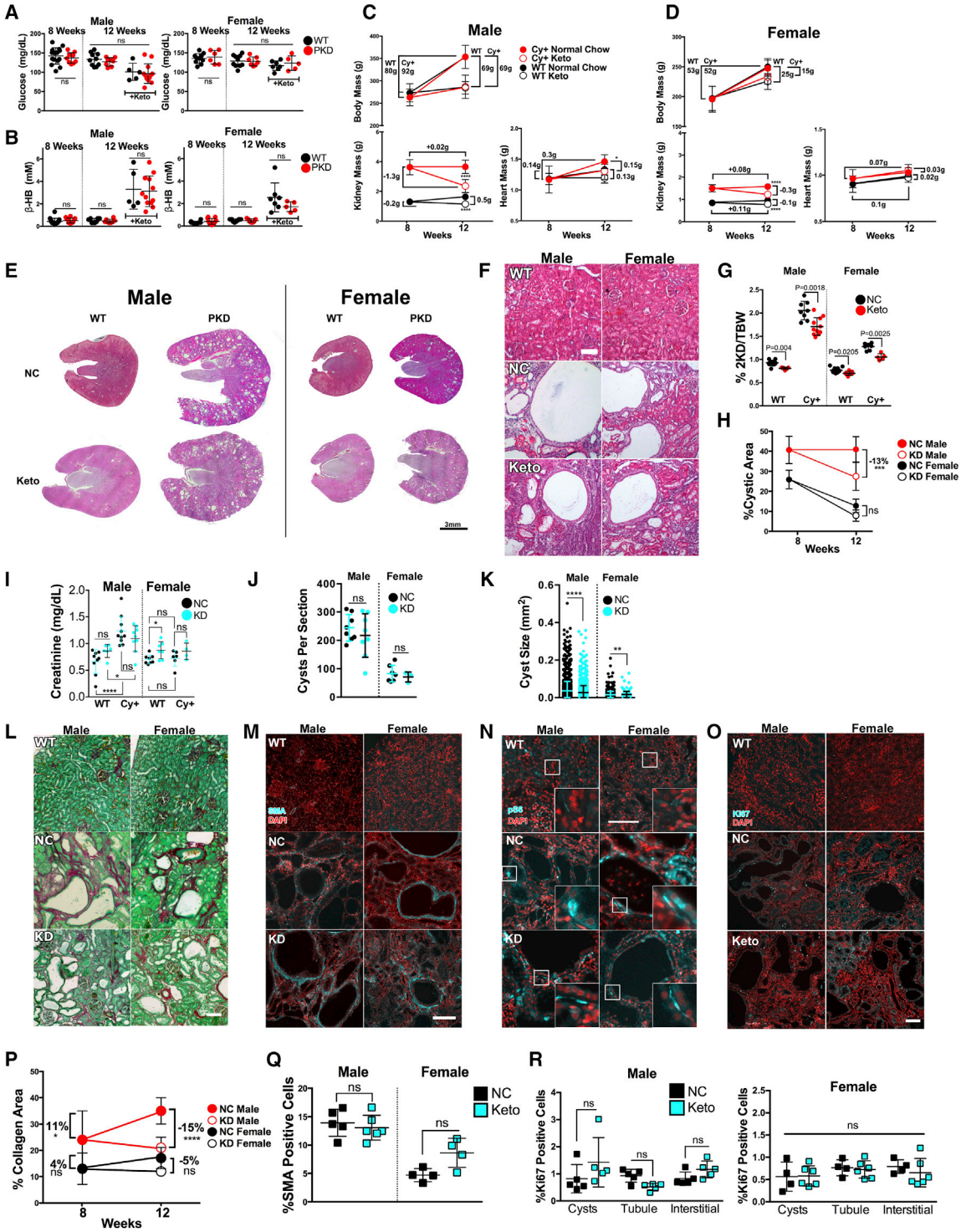

Figure 5. The Ketogenic Diet Reverses Kidney Disease Progression in Adult Han:SPRD Rats

(A) Blood glucose levels at initial (week 8) and final time point (week 12) of the experiment.

(B) Blood β-hydroxybutyrate levels.

(C and D) Percentage change in NC- and KD-treated animal's body, kidney, and heart mass over the 4-week treatment period. Bracketed masses reflect the difference between 8-week and 12-week values or differences between NC and KD rats.

(E and F) H&E-stained kidney sections. Scale bars represent 3 mm or 100 μm, respectively.

(G) 2-kidney to body weight ratios.

(H) Cystic index (percent cystic area).

(legend continued on next page)

only partially resolved to date (Newman and Verdin, 2017; Rojas-Morales et al., 2016). Importantly, BHB affects numerous signaling pathways that are implicated in PKD including mTOR, AMPK, and HDACs (Bartmann et al., 2018; Shimazu et al., 2013). To investigate whether BHB may have a dominant beneficial effect on PKD progression, we treated Han:SPRD rats with BHB from post-natal weeks 3–8 in the context of *ad libitum* feeding with normal, high-carbohydrate chow (NC). BHB was administered as a sodium and potassium salt in the drinking water *ad libitum* at a dose equivalent to that recommended as a dietary supplement in BHB supplement drinks. Control cohorts received either normal water or water supplemented with the molar equivalents of salt provided in the BHB supplement (a mixture of NaCl/KCl). All treated animals consumed comparable amounts of water and calories (Figure S7, related to Figure 7), and BHB treatment had no effect on body weight (Figure 7D) or blood glucose levels (Figure S7).

After 5 weeks of treatment with BHB, the kidneys of PKD animals were nearly indistinguishable from kidneys of wild-type animals, both at the gross and histological level (Figures 7A and 7B). BHB-treated PKD rats showed striking reductions in the 2-kidney to body weight ratio (Figure 7C) and the cystic area (Figure 7E) compared to water- and salt-treated controls. Neither wild-type kidneys nor other organs were affected by BHB treatment, indicating that the effect is specific to polycystic kidneys (Figure S7). BHB treatment led to a strong reduction in fibrosis (Figures 7B and 7G), almost complete elimination of myofibroblasts (Figure 7J), improved kidney function (Figure 7F), and inhibition of proliferation (Figures 7H and 7I).

These results demonstrate that BHB acts in a dominant fashion as a suppressor of PKD progression, even in animals that are fed a high-carbohydrate diet and have unaltered blood glucose levels. Altogether, our results suggest that inducing a state of ketosis, either by dietary intervention or by mimicking its effects with BHB, may be an effective treatment for ADPKD in humans.

Perspectives

Previous studies have suggested potential beneficial effects of lowering protein intake or changing the dietary protein composition in individuals with ADPKD (Klahr et al., 1995) and PKD rodent models (Devassy et al., 2017; Fair et al., 2004; Ogborn and Sareen, 1995; Tomobe et al., 1994). In most of these studies, the level of protein alteration was relatively major, but the beneficial effect was relatively minor. Protein alterations cannot account for the effects observed in our study because neither the amount nor composition of dietary protein was altered in our TRF regimen or in BHB treatment experiments. A potential mechanism that has been proposed to explain effects of TRF regimens is alteration in circadian rhythms. Again, such a mechanism cannot account for the effects observed here because the KD and BHB were administered *ad libitum*. Furthermore, TRF regimens were recently shown to be still effective in animals lacking a functional circadian clock (Chaix et al., 2018).

The sum of our results suggests that the metabolic changes induced during ketosis are responsible for suppressing PKD progression, likely by inhibiting both cystogenesis and cyst expansion. The main metabolic changes during ketosis are reflected in a shift of fuel source utilization: (1) decreased glucose availability, (2) increased fatty acid supply, and (3) increased ketone body supply. It is possible that a combination of all three factors contributes to the beneficial effect. PKD cells have been shown to have an altered cellular metabolism in which the preferred fuel source is glucose that is primarily metabolized by glycolysis, resembling a Warburg-like effect (Magistroni and Boletta, 2017). This phenotype might be caused by, or amplified by, recently observed mitochondrial defects that may impair the efficiency of the mitochondrial tricarboxylic acid (TCA) cycle and fatty acid β-oxidation (Ishimoto et al., 2017). This could lead to overall metabolic inflexibility that may lock PKD cells in a dependency on glucose and glycolysis. This view is consistent with the recently reported efficacy of the glycolysis inhibitor 2-DG in PKD mouse models (Magistroni and Boletta, 2017). Similarly, in our experiments, the TRF and KD regimens led to decreased blood glucose levels, which may have contributed to the observed inhibition of PKD progression. However, the effect of TRF on blood glucose was relatively minor. Furthermore, blood glucose was unaffected in our BHB treatment experiment. These results suggest that limiting the supply of glucose may be a contributing factor to the efficacy of ketosis but is not a requirement.

A common factor in all of the interventions carried out here is the elevation of BHB. TRF, KD, and acute fasting all raise BHB levels to varying degrees. Remarkably, treatment with BHB alone, even in the context of a normal high-carbohydrate rodent diet proved to be highly effective. This suggests that BHB itself is a major factor in suppressing PKD progression. There are two plausible mechanisms to explain this effect: BHB may affect PKD cells either as a metabolite or as a signaling molecule. As a metabolite, BHB is known for its favorable use in the TCA cycle by replacing succinyl-CoA and increasing the free pool of succinate, improving mitochondrial efficiency and TCA cycle turnover (Henderson, 2008; Veech et al., 2001). This may alter the overall metabolism of PKD cells and affect their ability to proliferate. On the other hand, BHB has numerous effects on signaling pathways, some of which have been implicated in PKD including

(I) Serum creatinine.
(J) Total number of cysts per kidney section.
(K) Cyst sizes of cysts counted in (J).
(L) Sirius red/Fast-Green-stained kidney sections showing collagen (red).
(M) SMA immunostaining (cyan).
(N) Immunostaining of the mTORC1 marker $pS6^{S235/236}$ (cyan).
(O) Ki-67 immunostaining.
(P) Quantification of collagen-positive area from animals in L and compared to 8-week rats.
(Q) Quantification of SMA-positive cells as a percent of the total number of cells.
(R) Quantification of Ki-67-positive cells separated by location into cyst lining, tubular, or interstitial and expressed as a percent of the total number of DAPI-stained nuclei. Scale bars represent 100 μm. Error bars represent SD. Statistical significance was determined using Mann-Whitney analysis. n = 12 male and 10 female cystic rats; n = 10 male and 14 female wild-type rats for adult ketogenic diet experiments. (*$p < 0.05$, ****$p < 0.0001$).

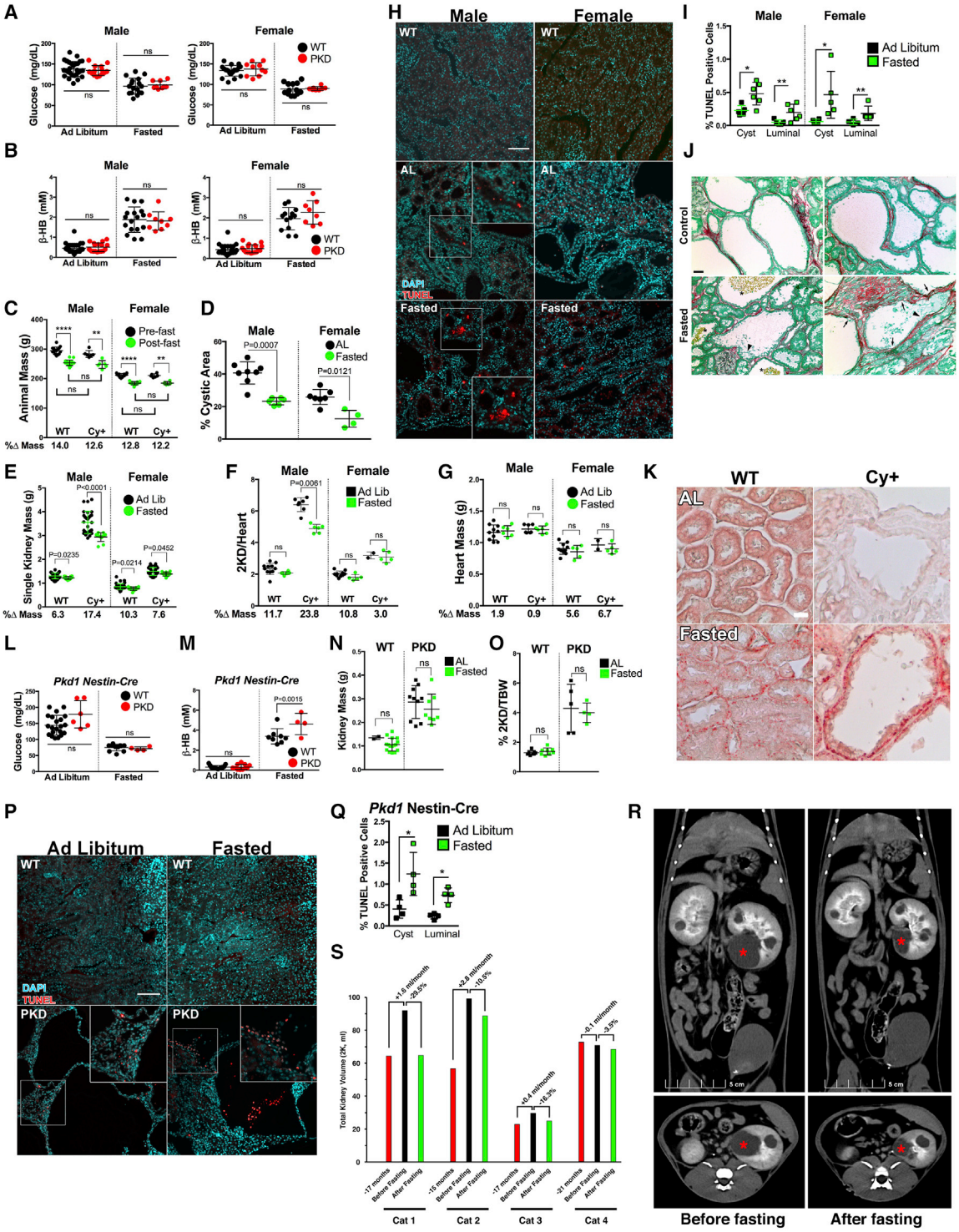

Figure 6. Acute Fasting Leads to Rapid Cystic Cell Death and Reduced Cyst and Kidney Size in Polycystic Kidneys

(A and B) (A) Blood glucose and (B) β-hydroxybutyrate levels of untreated and 48-h fasted Han:SPRD and WT rats.

(C) Animal mass.

(D) Cystic index (percent cystic area).

(E) Single kidney masses.

(F) 2-kidney to heart mass ratios.

(G) Heart masses.

(H) TUNEL stain. Kidneys from WT rats did not demonstrate significant levels of apoptosis. Scale bar represents 100 μm.

(legend continued on next page)

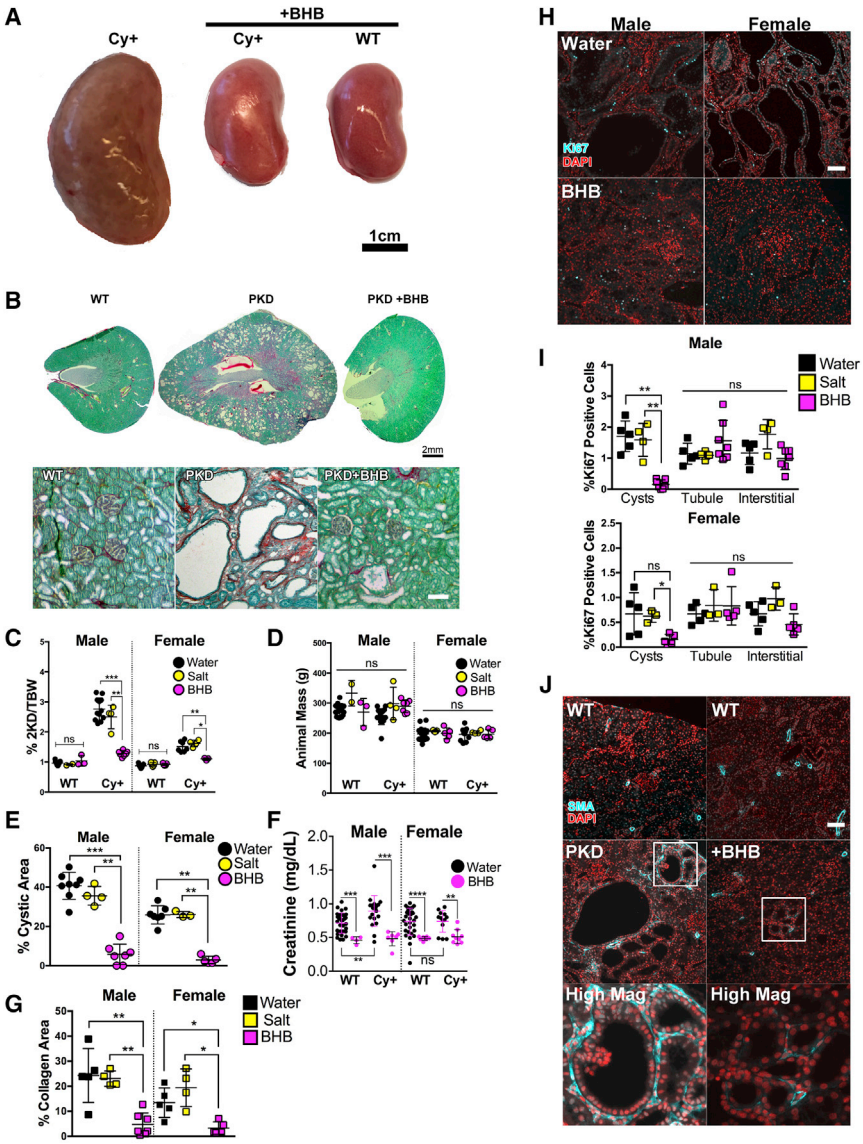

Figure 7. BHB Administration Ameliorates Disease Progression in the Han:SPRD Rat Model of PKD

(A) Gross kidney images of untreated cystic (left), BHB-treated cystic (middle), and BHB-treated wild-type (right) rats. Scale bar represents 1 cm.

(B) Sirius red/Fast-Green-stained kidney sections. Scale bar represents 2 mm and 50 μm, respectively.

(C–E) (C) 2-kidney to body weight ratios, (D) animal masses, and (E) cystic areas of water-, salt-, and BHB-treated rats.

(F) Serum creatinine.

(G) Percent collagen area from Sirius red/Fast-Green-stained sections.

(H) Ki-67 immunofluorescence stain.

(I) Ki-67 quantification.

(J) SMA immunofluorescence stain for myofibroblasts (cyan). Scale bar represents 50 μm. Error bars represent SD. Statistical significance was determined using Mann-Whitney analysis. n = 7 male and 5 female cystic rats; n = 3 male and n = 5 female wild-type rats treated with BHB and n = 4 male and 4 female cystic rats; n = 2 male and 5 female wild-type rats treated with Na/K salt. (*p < 0.05, **p < 0.01, ***p < 0.001).

mTOR, AMPK and HDACs (Bartmann et al., 2018; Newman and Verdin, 2017; Rojas-Morales et al., 2016; Shimazu et al., 2013). Therefore, BHB may affect PKD cells independent of its own metabolism. BHB has been identified as the endogenous ligand of the G-protein coupled receptor GPR109A, which is also activated by unphysiologically high concentrations of the vitamin niacin (Ristic et al., 2017). Interestingly, administration of megadoses of niacinamide has previously been shown to ameliorate PKD in a *Pkd1* mouse model, although the effect was believed to be due to direct inhibition of SIRT1 activity (Zhou et al., 2013). We speculate that both mega-concentrations of niacin and physiologically relevant concentrations of BHB, as they occur during ketosis, may inhibit PKD progression due to activation of GPR109A. GPR109A signals via inhibition of cAMP (Ristic et al., 2017), and aberrant cAMP signaling is a known driver of PKD progression (Chebib and

(I) Percentage of TUNEL-positive cells as the percent of the total number of DAPI-stained nuclei in cystic epithelia, tubules, interstitial, or cells within lumen.

(J) Sirius red/Fast Green stain of *ad libitum* and fasted Han:SPRD rats indicating collagen and basement membranes in red. Arrowheads denote fragmented epithelial cells. Arrows denote denuded epithelium. Asterisks denote red blood cells in cysts.

(K) Oil O Red stain. Scale bar represents 50 μm.

(L and M) (L) Blood glucose values and (M) BHB levels from 24-h fasted *Pkd1*$^{cond/cond}$:Nes^{cre} mice.

(N) Single kidney mass of AL and fasted *Pkd1*$^{cond/cond}$:Nes^{cre} mice.

(O) 2-kidney to body weight ratio of AL and fasted *Pkd1*$^{cond/cond}$:Nes^{cre} mice.

(P) TUNEL stain of kidney sections from *Pkd1*$^{cond/cond}$:Nes^{cre} mice after a 24-h fast. Scale bars represent 100 μm.

(Q) Percentage of TUNEL-positive epithelial cells or cells within cyst lumens as a percent of the total number of DAPI-stained nuclei in AL versus fasted *Pkd1*$^{cond/cond}$:Nes^{cre} mice in cystic.

(R) CT scans of PKD cats before and after 72 h fast. * Denotes the same cyst in each image.

(S) Quantification of total kidney volumes of PKD cats determined ~1.5 years prior to the study, immediately before fasting or immediately after fasting. Error bars represent SD. Statistical significance was determined using Mann-Whitney analysis. n = 8 male and 5 female cystic rats; n = 7 male and 5 female wild-type rats, n = 4 polycystic cats, and n = 4 female cystic *Pkd1*$^{cond/cond}$:Nes^{cre} mice; n = 3 male and 5 female wild-type mice were used for fasting experiments. *p < 0.05, **p < 0.01, ****p < 0.0001).

Torres, 2018; Cornec-Le Gall et al., 2019). Future work is needed to elucidate the mechanism of BHB action in PKD.

Another possible mechanism by which ketosis may contribute to the inhibition of PKD progression involves the increased supply of fatty acids released by the adipose tissue. We show that acute fasting leads to an extreme level of lipid loading in cyst-lining epithelial cells. This suggests that these cells are fully capable of taking up circulating fatty acids but appear to be unable to catabolize them, which necessitates their deposition into lipid droplets as a stress response similar to what has been observed in cancer cells (Petan et al., 2018). During acute fasting, which leads to a rapid onset of ketosis, the ability of PKD cells to sequester fatty acids in lipid droplets may be overwhelmed leading to lipotoxicity and cell death. This mechanism is consistent with the greater cell death, cyst rupture, and draining of cyst fluid that we observed as a rapid response to acute fasting. This view is also consistent with the previously described defect of fatty acid oxidation in PKD (Lakhia et al., 2018; Menezes et al., 2016) that can lead to increased lipid loading in PKD cells *in vitro* (Lin et al., 2018).

Our results show that ketosis strongly inhibits not only renal cyst growth but also fibrosis. During the progression of PKD, cyst proliferation and fibrosis typically go hand in hand, and it is likely that both processes reinforce each other. Myofibroblasts have been shown to be abundant in PKD kidneys and are thought to be a major contributor to fibrosis (Norman, 2011). We find that ketosis greatly reduces the abundance of pericystic myofibroblasts, especially the TRF regimen and BHB treatment, to almost complete absence. Consequently, overall fibrosis, as measured by collagen deposition, is strongly reduced. Future studies are required to determine whether the primary effect of ketosis is on cyst-lining epithelial cells or on myofibroblasts or on both simultaneously.

The KD regimen that we employed to force animals into sustained ketosis utilized a standard high-fat, very-low-carbohydrate diet. This regimen was highly effective in preventing PKD progression, which may be surprising in light of previous reports that increases in dietary fat intake worsened PKD progression in the Han:SPRD rat model (Jayapalan et al., 2000) and in *Pkd1* mouse models (Menezes et al., 2016). However, in those studies, the fat contents were altered in the context of a high-carbohydrate food background, which would prevent animals from experiencing ketosis.

We have investigated different interventions to induce ketosis—TRF, KD, acute fasting, and direct oral BHB administration—using multiple PKD models: the non-orthologous Han:SPRD rat model, the orthologous *Pkd1* mouse model, and the orthologous feline ADPKD model. These multiple approaches all led to consistent results, which suggests that the observed effects are predictive for human ADPKD.

The main significance of our findings lies in the almost immediate clinical applicability and the suggestion that effective ADPKD therapy may be possible by dietary intervention and without the need for pharmacological intervention. Although head-to-head comparisons would have to be made, in our experience, the magnitude of the observed beneficial effect of ketosis on PKD progression appears to be greater than the effect of any pharmacological compound that has been tested in rodent models of PKD to date. This includes effects of vasopressin V2 receptor antagonists (Gattone et al., 2003) that eventually led to the first—and only—approved drug therapy for ADPKD. This drug, tolvaptan, was shown to be modestly effective in clinical trials (Torres et al., 2012), but its use is complicated due to side effects including polyuria and potential liver toxicity (Chebib and Torres, 2018), and its high cost has called the cost-effectiveness into question (Erickson et al., 2013). In contrast, dietary interventions to induce ketosis, such as fasting, are not costly and appear relatively safe. Fasting is a long-held practice for both health and religious purposes in many cultures dating back to prehistoric times and may perhaps be considered the oldest form of medical therapy. It has recently been reported that fasting during the month of Ramadan, a form of time-restricted diet, has no negative effects on renal function in individuals with ADPKD (Ekinci et al., 2018). The KD has been clinically used as an effective and safe therapy for pediatric epilepsy for nearly 100 years (Huffman and Kossoff, 2006). While this diet is also widely used to control obesity and diabetes, even among lay people, it is important to note that it is not necessarily free of side effects and should be supervised by a physician. KDs are contraindicated in the presence of certain rare genetic metabolic disorders and can also lead to an increased risk of kidney stones (Kossoff et al., 2018). The latter may be a particular concern in the case of ADPKD.

Unfortunately, dietary interventions most frequently fail as therapies due to inability of individuals to adhere to the diets. Our finding that oral treatment with BHB alone, on top of the normal *ad libitum*-fed high-carbohydrate diet, was highly effective in halting PKD progression suggests that a similar treatment would be feasible in individuals with ADPKD. BHB is readily available in the US as a dietary supplement. We administered BHB with the drinking water mimicking the dose that manufacturers of sports and energy supplements recommend. Such supplementation would avoid the need for lifestyle changes required for time-restricted diets or KDs, greatly increasing feasibility.

Most individuals with ADPKD in industrialized societies consume a high-carbohydrate diet throughout their waking hours and only rarely, if ever, experience periods of ketosis. A recent nutritional feasibility study recommends high-carbohydrate diets for individuals with ADPKD (Taylor et al., 2017) as do many available cookbooks, websites, online forums, etc., where individuals with ADPKD may seek dietary advice. Our results suggest that such dietary habits may worsen PKD progression. This concept is also supported by a recent report of faster disease progression in overweight and obese early-stage ADPKD (Nowak et al., 2018). Moderation in caloric intake has sensibly been recommended for the management of ADPKD (Chebib and Torres, 2018). Our results presented here suggest, however, that reducing caloric intake *per se* would not necessarily lead to inhibition of cystic progression but that the induction of the state of ketosis is instead important, irrespective of caloric intake. Rigorous validation of dietary recommendations in randomized clinical trials is urgently needed and may lead to scientifically validated dietary interventions with the potential to become the standard of care for ADPKD.

Limitations of Study

Several of the experiments in this study make use of the non-orthologous Han:SPRD rat model of PKD. The mutation in this

model affects a gene, samcystin, that is different from the PKD genes affected in human ADPKD, and it is unclear if and how samcystin may interact with the polycystins, the products of the PKD genes. Therefore, there is the caveat that results obtained in this model may not necessarily be predictive for the human disease. This caveat is balanced by the fact that the results obtained with this non-orthologous model are in agreement with results from other experiments in this study in which the orthologous *Pkd1* mouse model and the orthologous *Pkd1* feline model were used. Furthermore, the beneficial effect of dietary restriction—which we now suggest was due to ketosis—was originally observed by two independent laboratories—including ours—using altogether three different orthologous *Pkd1* or *Pkd2* mouse models (Kipp et al., 2016; Warner et al., 2016).

STAR★METHODS

Detailed methods are provided in the online version of this paper and include the following:

- KEY RESOURCES TABLE
- LEAD CONTACT AND MATERIALS AVAILABILITY
- EXPERIMENTAL MODEL AND SUBJECT DETAILS
  - Animals
- METHOD DETAILS
  - Histology and Immunofluorescence Microscopy
  - Oil O Red Staining
  - Immunofluorescence Staining
  - Myofibroblast Quantification
  - Ki-67 Quantification
  - Phospho-S6 Quantification
  - Cyst Size and Cyst Number Quantification
  - Immunoblotting
- QUANTIFICATION AND STATISTICAL ANALYSIS

SUPPLEMENTAL INFORMATION

Supplemental Information can be found online at https://doi.org/10.1016/j.cmet.2019.09.012.

ACKNOWLEDGMENTS

We thank Alyssa Sahu for help with experiments and Diego Acosta-Alvear for help with artwork. This work was supported by a grant from the National Institutes of Health (NIH; DK109563) and gifts from the Lillian Goldman Charitable Trust and the Amy P. Goldman Foundation to T.W., a Jarrett Postdoctoral Fellowship from the Jarrett Family Fund for work in T.W.'s laboratory, and the University of Missouri Gilbreath McLorn Endowment to L.A.L. M.M. was in part supported by a grant from the Office of Research and Development, Medical Research Service, Department of Veterans Affairs (1 I01 BX004232-01A2). The CRISP study is supported by cooperative agreements from the National Institute of Diabetes and Digestive and Kidney Diseases (NIDDK) of the NIH (DK056943, DK056956, DK056957, and DK056961) and by R01 DK113111. The CRISP study was also supported in part by the NIDDK through P30 grants to the Kansas PKD Research and Translation Core Center (DK106912), the Mayo Translational PKD Center (DK090728), and UAB Hepatorenal Fibrocystic Diseases Core Center (DK074038) and by the National Center for Research Resources General Clinical Research Centers at each institution (RR000039, Emory University; RR00585, Mayo College of Medicine; RR23940, Kansas University Medical Center; RR000032, University of Alabama at Birmingham), and the National Center for Advancing Translational Sciences Clinical and Translational Science Awards at each institution (RR025008 and TR000454, Emory; RR024150 and TR000135, Mayo College of Medicine; RR033179 and TR000001, Kansas University Medical Center; RR025777, TR000165, and TR001417, University of Alabama at Birmingham; RR024153 and TR000005, University of Pittsburgh School of Medicine).

AUTHOR CONTRIBUTIONS

J.A.T. contributed to experimental design, animal procedures, manuscript preparation, and data analysis. S.L.K. contributed to experiments. C.B., T.A., and S.A. contributed to data analysis and animal procedures. J.R.D. and L.A.L. contributed to experimental design, execution, and analysis of experiments on feline ADPKD. M.M. represented the Consortium for Radiologic Imaging Studies of Polycystic Kidney Disease that recruited the patient cohort, collected, and analyzed the data. T.W. acted as the principal investigator and contributed to the design and supervision of experiments, the preparation of figures and writing of the manuscript. All authors contributed to the interpretation of the data, revised the manuscript, and approved the final version.

DECLARATION OF INTERESTS

J.A.T. and T.W. are listed inventors on a provisional patent application filed by UCSB related to discoveries reported in this paper. T.W. is an inventor on a patent application by UCSB on a discovery unrelated to this paper. M.M. reports grants and consulting fees outside the submitted work from Otsuka Pharmaceuticals, Sanofi, and Chinook Therapeutics.

Received: April 26, 2019
Revised: July 22, 2019
Accepted: September 16, 2019
Published: October 17, 2019

REFERENCES

Bae, H.R., Kim, D.H., Park, M.H., Lee, B., Kim, M.J., Lee, E.K., Chung, K.W., Kim, S.M., Im, D.S., and Chung, H.Y. (2016). β-hydroxybutyrate suppresses inflammasome formation by ameliorating endoplasmic reticulum stress via AMPK activation. Oncotarget *7*, 66444–66454.

Bartmann, C., Janaki Raman, S.R., Flöter, J., Schulze, A., Bahlke, K., Willingstorfer, J., Strunz, M., Wöckel, A., Klement, R.J., Kapp, M., et al. (2018). Beta-hydroxybutyrate (3-OHB) can influence the energetic phenotype of breast cancer cells, but does not impact their proliferation and the response to chemotherapy or radiation. Cancer Metab. *6*, 8.

Brown, J.H., Bihoreau, M.T., Hoffmann, S., Kränzlin, B., Tychinskaya, I., Obermüller, N., Podlich, D., Boehn, S.N., Kaisaki, P.J., Megel, N., et al. (2005). Missense mutation in sterile alpha motif of novel protein SamCystin is associated with polycystic kidney disease in (cy/+) rat. J. Am. Soc. Nephrol. *16*, 3517–3526.

Chaix, A., Lin, T., Le, H.D., Chang, M.W., and Panda, S. (2018). Time-restricted feeding prevents obesity and metabolic syndrome in mice lacking a circadian clock. Cell Metab. *28*, 303–319.e4.

Chang, M.Y., Ma, T.L., Hung, C.C., Tian, Y.C., Chen, Y.C., Yang, C.W., and Cheng, Y.C. (2017). Metformin inhibits cyst formation in a zebrafish model of Polycystin-2 deficiency. Sci. Rep. *7*, 7161.

Chebib, F.T., and Torres, V.E. (2018). Recent advances in the management of autosomal dominant polycystic kidney disease. Clin. J. Am. Soc. Nephrol. *13*, 1765–1776.

Chiaravalli, M., Rowe, I., Mannella, V., Quilici, G., Canu, T., Bianchi, V., Gurgone, A., Antunes, S., D'Adamo, P., Esposito, A., et al. (2016). 2-Deoxy-d-glucose ameliorates PKD progression. J. Am. Soc. Nephrol. *27*, 1958–1969.

Chumley, P., Zhou, J., Mrug, S., Chacko, B., Parant, J.M., Challa, A.K., Wilson, L.S., Berryhill, T.F., Barnes, S., Kesterson, R.A., et al. (2018). Truncating PKHD1 and PKD2 mutations alter energy metabolism. Am. J. Physiol. Ren. Physiol. *316*, F414–F425.

Cornec-Le Gall, E., Alam, A., and Perrone, R.D. (2019). Autosomal dominant polycystic kidney disease. Lancet *393*, 919–935.

Cornu, M., Albert, V., and Hall, M.N. (2013). mTOR in aging, metabolism, and cancer. Curr. Opin. Genet. Dev. *23*, 53–62.

Cowley, B.D., Gudapaty, S., Kraybill, A.L., Barash, B.D., Harding, M.A., Calvet, J.P., and Gattone, V.H. (1993). Autosomal-dominant polycystic kidney disease in the rat. Kidney Int. *43*, 522–534.

Devassy, J.G., Yamaguchi, T., Monirujjaman, M., Gabbs, M., Ravandi, A., Zhou, J., and Aukema, H.M. (2017). Distinct effects of dietary flax compared to fish oil, soy protein compared to casein, and sex on the renal oxylipin profile in models of polycystic kidney disease. Prostaglandins Leukot. Essent. Fatty Acids *123*, 1–13.

Ekinci, I., Erkoc, R., Gursu, M., Dogan, E.E., Kilic, E., Cebeci, E., Ozturk, S., and Kazancioglu, R. (2018). Effects of fasting during the month of Ramadan on renal function in patients with autosomal dominant polycystic kidney disease. Clin. Nephrol. *89*, 103–112.

Erickson, K.F., Chertow, G.M., and Goldhaber-Fiebert, J.D. (2013). Cost-effectiveness of tolvaptan in autosomal dominant polycystic kidney disease. Ann. Intern. Med. *159*, 382–389.

Fair, D.E., Ogborn, M.R., Weiler, H.A., Bankovic-Calic, N., Nitschmann, E.P., Fitzpatrick-Wong, S.C., and Aukema, H.M. (2004). Dietary soy protein attenuates renal disease progression after 1 and 3 weeks in Han:SPRD-cy weanling rats. J. Nutr. *134*, 1504–1507.

Fedorov, A., Beichel, R., Kalpathy-Cramer, J., Finet, J., Fillion-Robin, J.C., Pujol, S., Bauer, C., Jennings, D., Fennessy, F., Sonka, M., et al. (2012). 3D Slicer as an image computing platform for the Quantitative Imaging Network. Magn. Reson. Imaging *30*, 1323–1341.

Flowers, E.M., Sudderth, J., Zacharias, L., Mernaugh, G., Zent, R., DeBerardinis, R.J., and Carroll, T.J. (2018). LKB1 deficiency confers glutamine dependency in polycystic kidney disease. Nat. Commun. *9*, 814.

Gatica, R., Bertinat, R., Silva, P., Kairath, P., Slebe, F., Pardo, F., Ramírez, M.J., Slebe, J.C., Campistol, J.M., Nualart, F., et al. (2015). Over-expression of muscle glycogen synthase in human diabetic nephropathy. Histochem. Cell Biol. *143*, 313–324.

Gattone, V.H., Wang, X., Harris, P.C., and Torres, V.E. (2003). Inhibition of renal cystic disease development and progression by a vasopressin V2 receptor antagonist. Nat. Med. *9*, 1323–1326.

Grabacka, M., Pierzchalska, M., Dean, M., and Reiss, K. (2016). Regulation of ketone body metabolism and the role of PPARα. Int. J. Mol. Sci. *17*.

Henderson, S.T. (2008). Ketone bodies as a therapeutic for Alzheimer's disease. Neurotherapeutics *5*, 470–480.

Huffman, J., and Kossoff, E.H. (2006). State of the ketogenic diet(s) in epilepsy. Curr. Neurol. Neurosci. Rep. *6*, 332–340.

Hwang, V.J., Kim, J., Rand, A., Yang, C., Sturdivant, S., Hammock, B., Bell, P.D., Guay-Woodford, L.M., and Weiss, R.H. (2015). The cpk model of recessive PKD shows glutamine dependence associated with the production of the oncometabolite 2-hydroxyglutarate. Am. J. Physiol. Renal Physiol. *309*, F492–F498.

Ishimoto, Y., Inagi, R., Yoshihara, D., Kugita, M., Nagao, S., Shimizu, A., Takeda, N., Wake, M., Honda, K., Zhou, J., et al. (2017). Mitochondrial abnormality facilitates cyst formation in autosomal dominant polycystic kidney disease. Mol. Cell. Biol. *37*, 1–23.

Jayapalan, S., Saboorian, M.H., Edmunds, J.W., and Aukema, H.M. (2000). High dietary fat intake increases renal cyst disease progression in Han:SPRD-cy rats. J. Nutr. *130*, 2356–2360.

Kipp, K.R., Rezaei, M., Lin, L., Dewey, E.C., and Weimbs, T. (2016). A mild reduction of food intake slows disease progression in an orthologous mouse model of polycystic kidney disease. Am. J. Physiol. Renal Physiol. *310*, F726–F731.

Kipp, K.R., Kruger, S.L., Schimmel, M.F., Parker, N., Shillingford, J.M., Leamon, C.P., and Weimbs, T. (2018). Comparison of folate-conjugated rapamycin versus unconjugated rapamycin in an orthologous mouse model of polycystic kidney disease. Am. J. Physiol. Renal Physiol. *315*, F395–F405.

Klahr, S., Breyer, J.A., Beck, G.J., Dennis, V.W., Hartman, J.A., Roth, D., Steinman, T.I., Wang, S.R., and Yamamoto, M.E. (1995). Dietary protein restriction, blood pressure control, and the progression of polycystic kidney disease. Modification of Diet in Renal Disease Study Group. J. Am. Soc. Nephrol. *5*, 2037–2047.

Kossoff, E.H., Zupec-Kania, B.A., Auvin, S., Ballaban-Gil, K.R., Christina Bergqvist, A.G., Blackford, R., Buchhalter, J.R., Caraballo, R.H., Cross, J.H., Dahlin, M.G., et al. (2018). Optimal clinical management of children receiving dietary therapies for epilepsy: updated recommendations of the International Ketogenic Diet Study Group. Epilepsia Open *3*, 175–192.

Kraus, A., Schley, G., Kunzelmann, K., Schreiber, R., Peters, D.J.M., Stadler, R., Eckardt, K.U., and Buchholz, B. (2016). Glucose promotes secretion-dependent renal cyst growth. J. Mol. Med. *94*, 107–117.

Krzystanek, M., Pedersen, T.X., Bartels, E.D., Kjaehr, J., Straarup, E.M., and Nielsen, L.B. (2010). Expression of apolipoprotein B in the kidney attenuates renal lipid accumulation. J. Biol. Chem. *285*, 10583–10590.

Lakhia, R., Yheskel, M., Flaten, A., Quittner-Strom, E.B., Holland, W.L., and Patel, V. (2018). PPARα agonist fenofibrate enhances fatty acid β-oxidation and attenuates polycystic kidney and liver disease in mice. Am. J. Physiol. Renal Physiol. *314*, F122–F131.

Leonhard, W.N., van der Wal, A., Novalic, Z., Kunnen, S.J., Gansevoort, R.T., Breuning, M.H., de Heer, E., and Peters, D.J.M. (2011). Curcumin inhibits cystogenesis by simultaneous interference of multiple signaling pathways: in vivo evidence from a Pkd1-deletion model. Am. J. Physiol. Renal Physiol. *300*, F1193–F1202.

Lin, C.C., Kurashige, M., Liu, Y., Terabayashi, T., Ishimoto, Y., Wang, T., Choudhary, V., Hobbs, R., Liu, L.K., Lee, P.H., et al. (2018). A cleavage product of Polycystin-1 is a mitochondrial matrix protein that affects mitochondria morphology and function when heterologously expressed. Sci. Rep. *8*, 2743.

Liśkiewicz, A.D., Kasprowska-Liśkiewicz, D., Sługocka, A., Nowacka-Chmielewska, M.M., Wiaderkiewicz, J., Jędrzejowska-Szypułka, H., Barski, J.J., and Lewin-Kowalik, J. (2018). The modification of the ketogenic diet mitigates its stunting effects in rodents. Appl. Physiol. Nutr. Metab. *43*, 203–210.

Lyons, L.A., Biller, D.S., Erdman, C.A., Lipinski, M.J., Young, A.E., Roe, B.A., Qin, B., and Grahn, R.A. (2004). Feline polycystic kidney disease mutation identified in PKD1. J. Am. Soc. Nephrol. *15*, 2548–2555.

Magistroni, R., and Boletta, A. (2017). Defective glycolysis and the use of 2-deoxy-glucose in polycystic kidney disease: from animal models to humans. J. Nephrol. *30*, 511–519.

Menezes, L.F., Lin, C.-C., Zhou, F., and Germino, G.G. (2016). Fatty acid oxidation is impaired in an orthologous mouse model of autosomal dominant polycystic kidney disease. EBioMedicine *5*, 183–192.

Newman, J.C., and Verdin, E. (2017). β-hydroxybutyrate: a signaling metabolite. Annu. Rev. Nutr. *37*, 51–76.

Norman, J. (2011). Fibrosis and progression of autosomal dominant polycystic kidney disease (ADPKD). Biochim. Biophys. Acta *1812*, 1327–1336.

Nowak, K.L., You, Z., Gitomer, B., Brosnahan, G., Torres, V.E., Chapman, A.B., Perrone, R.D., Steinman, T.I., Abebe, K.Z., Rahbari-Oskoui, F.F., et al. (2018). Overweight and obesity are predictors of progression in early autosomal dominant polycystic kidney disease. J. Am. Soc. Nephrol. *29*, 571–578.

Ogborn, M.R., and Sareen, S. (1995). Amelioration of polycystic kidney disease by modification of dietary protein intake in the rat. J. Am. Soc. Nephrol. *6*, 1649–1654.

Ong, A.C.M., and Harris, P.C. (2015). A polycystin-centric view of cyst formation and disease: the polycystins revisited. Kidney Int. *88*, 699–710.

Padovano, V., Kuo, I.Y., Stavola, L.K., Aerni, H.R., Flaherty, B.J., Chapin, H.C., Ma, M., Somlo, S., Boletta, A., Ehrlich, B.E., et al. (2017). The polycystins are modulated by cellular oxygen-sensing pathways and regulate mitochondrial function. Mol. Biol. Cell *28*, 261–269.

Petan, T., Jarc, E., and Jusović, M. (2018). Lipid droplets in cancer: guardians of fat in a stressful world. Molecules *23*.

Ravichandran, K., Zafar, I., He, Z., Doctor, R.B., Moldovan, R., Mullick, A.E., and Edelstein, C.L. (2014). An mTOR anti-sense oligonucleotide decreases polycystic kidney disease in mice with a targeted mutation in Pkd2. Hum. Mol. Genet. *23*, 4919–4931.

Reed, B., Helal, I., McFann, K., Wang, W., Yan, X.D., and Schrier, R.W. (2012). The impact of type II diabetes mellitus in patients with autosomal dominant polycystic kidney disease. Nephrol. Dial. Transplant. *27*, 2862–2865.

Ristic, B., Bhutia, Y.D., and Ganapathy, V. (2017). Cell-surface G-protein-coupled receptors for tumor-associated metabolites: A direct link to mitochondrial dysfunction in cancer. Biochim. Biophys. Acta *1868*, 246–257.

Riwanto, M., Kapoor, S., Rodriguez, D., Edenhofer, I., Segerer, S., and Wüthrich, R.P. (2016). Inhibition of aerobic glycolysis attenuates disease progression in polycystic kidney disease. PLoS One *11*, e0146654.

Rojas-Morales, P., Tapia, E., and Pedraza-Chaverri, J. (2016). β-hydroxybutyrate: a signaling metabolite in starvation response? Cell. Signal. *28*, 917–923.

Rowe, I., Chiaravalli, M., Mannella, V., Ulisse, V., Quilici, G., Pema, M., Song, X.W., Xu, H., Mari, S., Qian, F., et al. (2013). Defective glucose metabolism in polycystic kidney disease identifies a new therapeutic strategy. Nat. Med. *19*, 488–493.

Sas, K.M., Yin, H., Fitzgibbon, W.R., Baicu, C.F., Zile, M.R., Steele, S.L., Amria, M., Saigusa, T., Funk, J., Bunni, M.A., et al. (2015). Hyperglycemia in the absence of cilia accelerates cystogenesis and induces renal damage. Am. J. Physiol. Renal Physiol. *309*, F79–F87.

Saxton, R.A., and Sabatini, D.M. (2017). MTOR signaling in growth, metabolism, and disease. Cell *168*, 960–976.

Scerbo, D., Son, N.H., Sirwi, A., Zeng, L., Sas, K.M., Cifarelli, V., Schoiswohl, G., Huggins, L.A., Gumaste, N., Hu, Y., et al. (2017). Kidney triglyceride accumulation in the fasted mouse is dependent upon serum free fatty acids. J. Lipid Res. *58*, 1132–1142.

Serra, A.L., Poster, D., Kistler, A.D., Krauer, F., Raina, S., Young, J., Rentsch, K.M., Spanaus, K.S., Senn, O., Kristanto, P., et al. (2010). Sirolimus and kidney growth in autosomal dominant polycystic kidney disease. N. Engl. J. Med. *363*, 820–829.

Shillingford, J.M., Murcia, N.S., Larson, C.H., Low, S.H., Hedgepeth, R., Brown, N., Flask, C.A., Novick, A.C., Goldfarb, D.A., Kramer-Zucker, A., et al. (2006). The mTOR pathway is regulated by polycystin-1, and its inhibition reverses renal cystogenesis in polycystic kidney disease. Proc. Natl. Acad. Sci. USA *103*, 5466–5471.

Shillingford, J.M., Piontek, K.B., Germino, G.G., and Weimbs, T. (2010). Rapamycin ameliorates PKD resulting from conditional inactivation of Pkd1. J. Am. Soc. Nephrol. *21*, 489–497.

Shimazu, T., Hirschey, M.D., Newman, J., He, W., Shirakawa, K., Le Moan, N.L., Grueter, C.A., Lim, H., Saunders, L.R., Stevens, R.D., et al. (2013). Suppression of oxidative stress by β-hydroxybutyrate, an endogenous histone deacetylase inhibitor. Science *339*, 211–214.

Song, C.J., Zimmerman, K.A., Henke, S.J., and Yoder, B.K. (2017). Inflammation and fibrosis in polycystic kidney disease. In Kidney Development and Disease (Springer), pp. 323–344.

Takakura, A., Nelson, E.A., Haque, N., Humphreys, B.D., Zandi-Nejad, K., Frank, D.A., and Zhou, J. (2011). Pyrimethamine inhibits adult polycystic kidney disease by modulating STAT signaling pathways. Hum. Mol. Genet. *20*, 4143–4154.

Talbot, J.J., Shillingford, J.M., Vasanth, S., Doerr, N., Mukherjee, S., Kinter, M.T., Watnick, T., and Weimbs, T. (2011). Polycystin-1 regulates STAT activity by a dual mechanism. Proc. Natl. Acad. Sci. USA *108*, 7985–7990.

Talbot, J.J., Song, X., Wang, X., Rinschen, M.M., Doerr, N., LaRiviere, W.B., Schermer, B., Pei, Y.P., Torres, V.E., and Weimbs, T. (2014). The cleaved cytoplasmic tail of polycystin-1 regulates Src-dependent STAT3 activation. J. Am. Soc. Nephrol. *25*, 1737–1748.

Taylor, J.M., Hamilton-Reeves, J.M., Sullivan, D.K., Gibson, C.A., Creed, C., Carlson, S.E., Wesson, D.E., and Grantham, J.J. (2017). Diet and polycystic kidney disease: a pilot intervention study. Clin. Nutr. *36*, 458–466.

Tomobe, K., Philbrick, D., Aukema, H.M., Clark, W.F., Ogborn, M.R., Parbtani, A., Takahashi, H., and Holub, B.J. (1994). Early dietary protein restriction slows disease progression and lengthens survival in mice with polycystic kidney disease. J. Am. Soc. Nephrol. *5*, 1355–1360.

Torres, V.E., Chapman, A.B., Devuyst, O., Gansevoort, R.T., Grantham, J.J., Higashihara, E., Perrone, R.D., Krasa, H.B., Ouyang, J., Czerwiec, F.S., et al. (2012). Tolvaptan in patients with autosomal dominant polycystic kidney disease. N. Engl. J. Med. *367*, 2407–2418.

Torres, J.A., Rezaei, M., Broderick, C., Lin, L., Wang, X., Hoppe, B., Cowley, B.D., Savica, V., Torres, V.E., Khan, S., et al. (2019). Crystal deposition triggers tubule dilation that accelerates cystogenesis in polycystic kidney disease. J. Clin. Invest. *130*.

Veech, R.L., Chance, B., Kashiwaya, Y., Lardy, H.A., and Cahill, G.F. (2001). Ketone bodies, potential therapeutic uses. IUBMB Life *51*, 241–247.

Wahl, P.R., Serra, A.L., Le Hir, M., Molle, K.D., Hall, M.N., and Wüthrich, R.P. (2006). Inhibition of mTOR with sirolimus slows disease progression in Han:SPRD rats with autosomal dominant polycystic kidney disease (ADPKD). Nephrol. Dial. Transplant. *21*, 598–604.

Walz, G., Budde, K., Mannaa, M., Nürnberger, J., Wanner, C., Sommerer, C., Kunzendorf, U., Banas, B., Hörl, W.H., Obermüller, N., et al. (2010). Everolimus in patients with autosomal dominant polycystic kidney disease. N. Engl. J. Med. *363*, 830–840.

Warner, G., Hein, K.Z., Nin, V., Edwards, M., Chini, C.C.S., Hopp, K., Harris, P.C., Torres, V.E., and Chini, E.N. (2016). Food restriction ameliorates the development of polycystic kidney disease. J. Am. Soc. Nephrol. *27*, 1437–1447.

Weimbs, T., Olsan, E.E., and Talbot, J.J. (2013). Regulation of STATs by polycystin-1 and their role in polycystic kidney disease. JAKSTAT *2*, e23650.

Weimbs, T., Shillingford, J.M., Torres, J., Kruger, S.L., and Bourgeois, B.C. (2018). Emerging targeted strategies for the treatment of autosomal dominant polycystic kidney disease. Clin. Kidney J. *11*, i27–i38.

Yu, A.S.L., Shen, C., Landsittel, D.P., Grantham, J.J., Cook, L.T., Torres, V.E., Chapman, A.B., Bae, K.T., Mrug, M., Harris, P.C., et al. (2019). Long-term trajectory of kidney function in autosomal-dominant polycystic kidney disease. Kidney Int. *95*, 1253–1261.

Zhou, X., Fan, L.X., Sweeney, W.E., Denu, J.M., Avner, E.D., and Li, X. (2013). Sirtuin 1 inhibition delays cyst formation in autosomal-dominant polycystic kidney disease. J. Clin. Invest. *123*, 3084–3098.

STAR★METHODS

KEY RESOURCES TABLE

REAGENT or RESOURCE	SOURCE	IDENTIFIER
Antibodies		
Anti-Phospho-S6 Ribosomal Protein (Ser235/236) (D57.2.2E) XP Rabbit mAb	Cell Signaling	Cat#4858; RRID: AB_2721245
Anti-Smooth Muscle Actin (1A4) Mouse mAb	Sigma-Aldrich	Cat#A5228; RRID: AB_262054
Anti-Ki-67 Rabbit pAb	EMD Millipore	Cat#AB9260; RRID: AB_2142366
Anti-Phospho-STAT3 (Tyr705) (D3A7) XP Rabbit mAb	Cell Signaling	Cat#9145; RRID: AB_2491009
Anti-Rabbit IgG (H+L) Secondary Goat Ab, DyLight 488	ThermoFisher	Cat#35552; RRID: AB_844398
Anti-Rabbit IgG (H+L) Secondary Goat Ab, DyLight 594	ThermoFisher	Cat#35560; RRID: AB_1185570
Anti-Mouse IgG (H+L) Secondary Goat Ab, DyLight 488	ThermoFisher	Cat#35502; RRID: AB_844397
Anti-Actin mAb (AC-15)	Amersham Bioscience	Cat#N350
Anti-Phospho-AMPKα (Thr172) (40H9) Rabbit mAb	Cell Signaling	Cat#2535; RRID: AB_331250
Anti-AMPKα (F6) Mouse mAb	Cell Signaling	Cat#2793
Anti-CPT1α (8F6AE9) Mouse mAb	Abcam	Cat#ab128568; RRID: AB_11141632
Chemicals, Peptides, and Recombinant Proteins		
Oil O Red (1-([4-(Xylylazo)xylyl]azo)-2-naphthol, 1-[2,5-Dimethyl-4-(2,5-dimethylphenylazo)phenylazo]-2-naphthol, Solvent Red 27)	Sigma-Aldrich	Cat#O0625
Protease inhibitor Cocktail (ingredients listed below)	In house	N/A
Pepstatin 7.3mM	Chemicon	Cat#E19
Leupeptin 11.72mM	Chemicon	Cat#E18
Antipain 14.76mM	Chemicon	Cat#E13
Benzamidine 450mM	Sigma-Aldrich	Cat#12072
Trasylol 10000U/mL	Sigma-Aldrich	Cat#A6279
Phosphatase Inhibitor Cocktail 2	Sigma-Aldrich	Cat#P5726
Phosphatase Inhibitor Cocktail 3	Sigma-Aldrich	Cat#P0044
KetoForce BHB Salt	Ketosports	Cat#PTN1010/929/1501
Dexmedetomidine	Zoetis	CAS:104075-48-1
Antisedan Atipamezole Hydrochloride	Zoetis	PubChem CID:71310
Propofol	N/A	CAS:2078-54-8
Buprenorphine	N/A	CAS:52485-79-7
Alfaxalone	N/A	CAS:23930-19-0 PubChem ID: 104845
Omnipaque 350 Iohexol	GE Healthcare	CAS:66108-95-0
Msp1 Fast Digest	Thermo-Fisher	FD0544
Critical Commercial Assays		
DeadEnd Fluorometric TUNEL system	Promega	Cat#G3250
Experimental Models: Organisms/Strains		
Mouse: *Pkd1*$^{Cond/Cond}$ *Nestin-Cre*/(C57BL/6)	Shillingford et al., 2010	N/A
Rat: PKD Han:Sprague-Dawley	Cowley et al., 1993	N/A
Oligonucleotides		
Pkd1 Genotype sense primer: ATT GGA CAA TGC CTG TGG TGA GTG	This Paper	N/A
Pkd1 Genotype anti-sense primer: TCG TGT TCC CTT ACC AAC CCT CTT	This Paper	N/A
Cre Genotype sense primer: ATG CTG TTT CAC TGG TTA TGC GGC	This Paper	N/A

(*Continued on next page*)

Continued

REAGENT or RESOURCE	SOURCE	IDENTIFIER
Cre Genotype anti-sense primer: ACC AGC TTG CAT GAT CTC GGG TAT	This Paper	N/A
Anks6 (*Pkdr1*) Genotype sense primer: CTA GAA GCC TCA GTG ACC CC	Brown et al., 2005	N/A
Anks6 (*Pkdr1*) Genotype anti-sense primer: CAG CGT GTG AAC AAG GTA GG	Brown et al., 2005	N/A
Software and Algorithms		
FIJI ImageJ	National Institutes of Health	https://fiji.sc/
Prism 8	GraphPad	https://www.graphpad.com/scientific-software/prism/
3D Slicer software	Fedorov et al., 2012	http://www.slicer.org
Photoshop CS5	Adobe	N/A
Other		
Aquillion 64 Imager	Canon Medical Systems	https://us.medical.canon/
Pico Lab Rodent Diet 20 5R53	LabDiet	Cat#3002890-742
Ketogenic Diet AIN-76A-Modified, High Fat, Paste	Bio-Serv	Cat#F3666
Teklad Custom Diet-Ketogenic Diet Very Low Protein (VLP)	Envigo	Cat#TD.110408
Persian Adult Dry Cat Food	Royal Canin	Cat#843507
Contour Next Blood Glucose Monitor	Bayer	Model#9628
Precision Xtra Blood Ketone Montior	Abbott	SKU#9881465

LEAD CONTACT AND MATERIALS AVAILABILITY

Further information and requests for resources and reagents should be directed to and will be fulfilled by the Lead Contact, Thomas Weimbs (weimbs@ucsb.edu).

EXPERIMENTAL MODEL AND SUBJECT DETAILS

Animals

All animal studies were conducted in accord with the National Research Council Guide with approval of the Institutional Animal Care and Use Committees at the respective institutions. Whenever possible and applicable, historical controls generated previously were used for comparison. Feline studies were conducted under University of Missouri (MU) IACUC approved protocol 9395. All animals were euthanized at the same time of day beginning at 10AM to control for effects that may be regulated by circadian rhythm and housed in a temperature controlled vivarium at 74°F +/-4°F on a 12-hour light/dark cycle. Cages are bedded with autoclaved Sani-chips and changed every 10-12 days for mice and every 7 days for rats. All animals were healthy at the time of euthanasia.

Pkd1$^{cond/cond}$:*Nes*^{cre} mice: *Pkd1* mice were group housed and separated by sex at weaning beginning at week 3 of age. These mice were described previously (Shillingford et al., 2010). *Pkd1*$^{cond/wt}$:*Nes*Cre$^{+/-}$ mice were bred with *Pkd1*$^{cond/cond}$:*Nes*$^{Cre-/-}$ mice to produce experimental cystic mice. Only female PKD mice were used during fasting experiments. Mice were genotyped using *Pkd1* primers as follows: sense primer: ATT GGA CAA TGC CTG TGG TGA GTG; anti-sense primer: TCG TGT TCC CTT ACC AAC CCT CTT. *Cre* primers as follows: sense primer: ATG CTG TTT CAC TGG TTA TGC GGC; anti-sense primer: ACC AGC TTG CAT GAT CTC GGG TAT.

Han:SPRD rats: Han:SPRD rats were obtained from the University of Oklahoma Health Sciences Center, courtesy of Dr. Benjamin Cowley, and a colony established at UCSB. Rats were group housed and given *ad libitum* access to food and water unless otherwise specified. Rats were weaned at 3 weeks of age and separated by sex. Rats were genotyped using a known polymorphism in the *Ansk6* (*Pkdr1*) gene coding for SamCystin. Heterozygous females were bred with wild-type males to reduce distressful phenotypes. PCR coupled to restriction digestion was used detect a C to T transition as described previously by Brown et al. (2005). DNA was extracted from a small piece of ear from each rat and PCR products were obtained from each DNA sample. Primers for rat SamCystin were as follows: sense primer: CTA GAA GCC TCA GTG ACC CC; anti-sense primer: CAG CGT GTG AAC AAG GTA GG. Amplification products were digested by Msp1 Fast Digest (Thermo-Fisher) at 37°C for 15 minutes. Digested PCR products were resolved on an agarose gel, producing bands at 157 and 85 bp; 242, 157, and 85 bp; and 242 bp for +/+, Cy/+, and Cy/Cy rats, respectively.

Time restricted feeding and ketogenic diet in juvenile PKD rats: Treatment of Han:SPRD (Cy/+) rats on a time-restricted diet began at postnatal week 3 until week 8 of age (n =8 male and 12 female Cy/+ rats; n =13 male and 8 female wild-type rats). Animals were

caged in cohorts between 2-6 rats and allowed water *ad libitum*. Animals were monitored daily for changes in behavior and for adverse effects of the diet. Food measurements and animal weights were performed daily. At weaning litters were separated by sex and then distributed randomly into group housing without consideration of genotype. Animals on a time-restricted diet received standard chow with a caloric ratio of ~62% carbohydrates, ~25% protein and ~13% fat, (Pico Lab Rodent Diet 20; LabDiet) for 8 hours daily starting 3 hours after beginning of the dark cycle. Animals (n =8 male and 7 female Cy+ rats; n =13 male and 6 female wild-type rats) on a ketogenic diet received ketogenic diet (#F3666 diet; Bio-Serv) comprised of a ~91% fat, ~2% carbohydrates and ~5% caloric ratio (See Table S2 for detailed information).

Ketogenic diet in adult PKD rats: Adult treatment began at week 8 until week 12 of age. Han:SPRD rats (n =12 male and 10 female cystic rats; n =10 male and 14 female wild-type rats) were fed *ad libitum* the pre-formulated ketogenic diet chow Envigo T.D. 110408 diet (Envigo) similar to ketogenic diet #F3666 but supplemented with 1.5g/kg methionine and 5g/kg choline (Table S2). Animals were monitored as described above.

Blood Measurements

Blood was collected via tail prick in all animals. Blood glucose was measured using a blood glucometer (Contour Next; Bayer), and β-hydroxybutyrate was measured using a blood ketone meter (Abbott; Precision Xtra). For TRF experiments, blood was collected prior to feeding after the 18 hour fasting period and is shown in Figures 1N, 1O, and S2. Acutely fasted and ad libitum access animal blood measurements were taken prior to sacrifice. Serum creatinine was measured using a creatinine assay kit (LifeSpan BioSciences; LS-K207).

Acute Rodent Fasting

Han:SPRD rats (n =8 male and 5 female cystic rats; n =7 male and 5 female wild-type rats), and *Pkd1*$^{cond/cond}$:Nes^{cre} mice (n =4 female cystic mice; n =3 male and 5 female wild-type mice) were fasted at 8 weeks of age for 48 or 24 hours, respectively, with *ad libitum* access to water. Animals were monitored for signs of distress during the treatment period. Water consumption was monitored daily.

ß-Hydroxybutyrate Supplementation in Rats

Treatment of Han:SPRD rats began at postnatal week 3 until week 8 of age (n =7 male and 5 female cystic rats; n =3 male and 5 female wild-type rats). Animals were caged in cohorts between 2-6 rats and allowed water *ad libitum*. Animals were monitored daily for changes in behavior and for adverse effects of the diet. Food and water measurements were recorded daily and animal weights recorded weekly. During the experiment, animals had *ad libitum* access to normal chow (Pico Lab 20). A BHB salt formulation (sodium/potassium, KetoForce; KetoSports) (n =7 male and 5 female cystic rats; n =3 male and n =5 female wild-type rats) delivered in the drinking water at 157.5mM BHB final concentration as previously used in rats (Chang et al., 2017), offered *ad libitum* and changed every 3 days or sooner if needed. The KetoForce solution is a BHB salt with 1.6g sodium and potassium per 11.7g BHB. Salt controls (n =4 male and 4 female cystic rats; n =2 male and 5 female wild-type rats) were treated with 2.24g:2.24g (1:1 mass ratio) sodium/potassium (from NaCl and KCl) supplemented water equivalent to the BHB solution.

Feline PKD Model

The cats were members of an ADPKD colony housed at the University of Missouri, Columbia. Cats were genotyped for the *PKD1* (10063C>A) mutation that causes feline ADPKD (Lyons et al., 2004). All cats were adult, ages ranged from 34.2-64.9 months, and were known to have cystic kidneys based on previous imaging diagnostics, including ultrasound, CT, and MRI (Table S3). Cats were fed Persian Adult dry cat food (Royal Canin; protein, min 28.0%; fat, min 20.0%; fiber, max 6.0%) *ad libitum*. Each cat had preliminary CT imaging ~1.5 years (15–21 months) prior to the study. Cats were fasted for at least 12 hours prior to the preliminary diagnostic imaging and placed under general anesthesia using clinical ansthetic protocols as deemed appropriate by the anesthesia service of the Veterinary Health Center ast MU. Alfaxalone (1-4 mg/kg IV or IM), dexmedetomidine (0.005-0.020 mg/kg IM) buprenorphine (0.005-0.01 mg/kg IM), Propofol (1-8 mg/kg) and isoflurane (inhaled to effect) were used in protocols for sedation/general anesthesia protocols.

All cats were intubated, and anesthesia was maintained using isoflurane gas, and a catheter was placed in the right brachial vein. For CT imaging during the fasting trial, the cats were sedated with 20 mg/kg dexmedetomidine (Zoetis, Parsippany, New Jersey), *i.m.* Cats were recovered from sedation with 350 - 400 mg/kg atipamezole (Zoetis), *i.m.* After the final post-fasting CT imaging, two cats were not recovered from sedation and euthanized by barbiturate overdose to obtain kidneys for pathological and histological examinations.

Two cats had ideal weight (body condition score (BCS = 5), one female was slightly overweight, and one cat was overweight (BCS = 7-8). Each cat was bright, alert and active during the entire fast and did not appear dehydrated, lethargic or depressed. Three cats lost 0.3 kg of weight but one cat had the same weight post-fasting.

All cats were healthy and had unremarkable CBC, serum chemistries and urinalyses. No cats had evidence of renal failure previously or at the time of the trial as based on creatinine, urine specific gravity and symmetrical dimethylarginine (SDMA) levels. All *PKD1* positive cats were clinically normal but due to the presence of cystic kidneys were classified as feline CKD Stage 1 (International Renal Interest Society; IRIS staging of CKD modified 2016; http://www.iris-kidney.com/guidelines/staging.html, accessed May 13, 2018).

Computed Tomography

CT imaging of cats was conducted using a third generation 64 slice instrument (Aquillion 64, Canon Medical Systems, Tustin, CA). Each cat was placed in dorsal recumbency and pre- and post-contrast images were obtained from the diaphragm to the anus (slice thickness 1–2 mm, kvp 80–100, mAs 230– 500). Intravenous non-ionic, iodinated contrast media (Omnipaque 350 Iohexol injection, GE Healthcare, Marlboro, MA.) was administered at a dose of 0.5 mg/kg and post-contrast images were obtained after a

three-minute delay. For the fasting study, cats were fasted for ~12 – 13 hrs prior to sedation for the pre-trial CT imaging. After the pre-trial CT, the fast was continued up to ~60 hrs. The cats were then re-sedated and the post-trial CT imaging and blood sampling was conducted. Total kidney volumes were determined by semi-automated volumetric segmentation using 3D Slicer software (http://www.slicer.org (Fedorov et al., 2012)) using the Segmentation Wizard module (author: Andrew Beers, Athinoula A. Martinos Center for Biomedical Imaging at Massachusetts General Hospital; available at: https://www.slicer.org/wiki/Documentation/Nightly/Extensions/SegmentationWizard, accessed 9 Apr. 2019).

METHOD DETAILS

Histology and Immunofluorescence Microscopy

Tissue embedding and histology: Tissues were removed and immediately placed into 4% paraformaldehyde for 24 hours then dehydrated through a decreasing alcohol series (2x 100%, 2x 95%, 2x 70%, 2x toluene) for 2 hours each and finally immersed in paraffin for 6 hours twice. Paraffin embedded tissues were then sectioned (5μm) and subjected to standard hematoxylin and eosin staining. To determine the cystic index, images of H&E sections were overlaid with a grid in Adobe Photoshop, and the intersection points on cysts vs. normal tissue were counted manually. To examine fibrosis, sections were deparaffinized and stained with 0.1% Sirius red and 0.1% Fast Green dissolved in picric acid on an orbital shaker, protected from light for 4 hours. Sections were then washed with tap water then dipped 10 times in increasing alcohol (95%, 100%) and cleared three times with xylene. Images were obtained for quantification by grid-overlay as described above. With the exclusion of blood vessels and absent tissue (e.g. Cysts), intersection points on Sirius red-positive structures were counted vs. total intersections.

Oil O Red Staining

Frozen sections were obtained by fixation of kidneys for 24 hours in formalin followed by incubation in 15% sucrose-PBS until tissues float, then incubation in 30% sucrose-PBS until tissues float again. Tissues were then placed in OCT imbedding compound (Fisher) and frozen using 100% ethanol in dry ice. 10μm sections were then cut and fixed with formalin. Sections were then rinsed in distilled water and washed with propylene glycol 2x 5 minutes followed by Oil O Red staining (0.7% (w/v) Oil O Red (Sigma-Aldrich) in propylene glycol) for 7 minutes with agitation. Sections were then incubated in 85% propylene glycol for 3 minutes, rinsed in distilled water and mounted using gelatin based aqueous mounting media (10g gelatin, 60ml distilled water, 70ml glycerol and 0.25g phenol; prepared in house).

Immunofluorescence Staining

Antigens were retrieved in 10 mM citrate-Na at pH 6.0 in a pressure cooker for 15 minutes. Slides were then blocked in (1% BSA, 0.1% fish skin gelatin, 0.1% sodium azide in TBST) at 37°C for 30 minutes. Sections were then treated with 0.1% Sudan Black in 70% ethanol for 20 minutes to reduce tissue auto fluorescence. After washing with TBST, slides were incubated in primary antibody overnight at 4°C. The following antibodies were used for immunostaining: Rabbit anti-pS6$^{S235/236}$, (#4858; Cell Signaling); Mouse-α-Smooth Muscle Actin (A5228; Sigma-Aldrich), Rabbit-Ki-67 (AB9260; EMD Millipore); Rabbit anti-pSTAT3^{Y705} (#9145; Cell Signaling). The sections were then incubated with species-specific fluorescently labeled secondary antibodies, diluted 1:200 in blocking buffer at 37°C for 1 hour. The following secondary antibodies were used for immunostaining: (Goat anti-Rabbit-DyLight 488 and 594, #35552 and #35560, ThermoFisher; goat anti-mouse-DyLight 488, ThermoFisher #35502). After washing in TBST, slides were post-fixed in neutral-buffered formalin for 10 minutes, washed in DI water and mounted with ProLong Gold antifade mounting medium with DAPI (ThermoFisher). The DeadEnd Fluorometric TUNEL system (Promega) was utilized for TUNEL staining and performed as specified by the manufacturer.

Myofibroblast Quantification

The prevalence of renal myofibroblasts was estimated by quantification of images stained for smooth muscle actin (SMA-1) with the exclusion of blood vessels. Grid intersection points on SMA-1 positive structures were counted vs. total intersections excluding non-tissue intersections.

Ki-67 Quantification

Ki-67 immunostained kidney sections were imaged and total number of DAPI positive nuclei were analyzed using FIJI (ImageJ; NIH) image software. At least 10 cortical areas were imaged and the number of Ki-67 positive cells were counted and parsed based on their location within the kidney. Percentages of Ki-67 positive cells are expressed as a fraction of the total counted nuclei.

Phospho-S6 Quantification

pS6 stained sections were imaged and analyzed for pS6 activity within cysts. Approximately 1000 cells were counted within cysts and the percentage of pS6 positive cells were expressed as a percentage of the total number of cells counted.

Cyst Size and Cyst Number Quantification

Whole kidney sections were imaged and the images were quantified using FIJI (ImageJ; NIH) image software. Individual cysts were counted and their sizes were recorded.

Immunoblotting

For sample preparation, kidneys were removed from euthanized animals, bisected and placed into a mortar cooled with liquid nitrogen, submersed in liquid nitrogen and pulverized using a pestle. These samples were then placed into microcentrifuge tubes and stored at -80°C for future analysis. Approximately 10mg of tissue were lysed in 200μL of 4% SDS-100mM Tris pH 6.8 lysis buffer containing phosphatase inhibitors (Phosphatase inhibitor cocktail 2 & 3 (Sigma-Aldrich) and protease inhibitor cocktail (Sigma-Aldrich). Samples were vortexed and heated at 100°C for 10 minutes followed by vortexing and centrifugation to pellet insoluble debris. Protein concentrations were estimated by reading the absorbance at 280nm using a NanoDrop spectrometer. Following standard SDS-PAGE and transfer onto nitrocellulose membranes, samples were analyzed using the following antibodies: Mouse anti-Actin (N350; Amersham Bioscience); Rabbit phopsho-AMPK^{Thr172} (#2535; Cell Signaling); Mouse total-AMPK, (#2793; Cell Signaling); Mouse anti-CPT1α, (#8F6AE9; Abcam).

QUANTIFICATION AND STATISTICAL ANALYSIS

The linear regression model analyses were performed with SAS 9.4 statistical software package (SAS Institute, Cary NC). Following tests for normal distribution, the statistical analyses were performed using Mann-Whitney unpaired one-tailed Student's t-test. Analysis was performed using Prism (GraphPad) software. Details for statistics can be found within the figure legends. PKD animals were housed with litter mates in groups between 2-4 animals without regard to genotype, resulting in a random distribution of PKD and wild-type animals in cohorts. Experimenters were not blinded to the treatment of genotypes of animals. The analysis of collagen, cystic index and smooth muscle actin images was conducted blinded. Exclusion criteria were based upon animal well-being. No animals were excluded from this study. No power analysis was done to determine sample sizes. Sample sizes were chosen based on experience with previous studies with PKD animals in our lab.